Spectrochimica Acta Part A: Molecular and Biomolecular Spectroscopy 349 (2026) 127375

Contents lists available at ScienceDirect

Spectrochimica Acta Part A:
Molecular and Biomolecular Spectroscopy

journal homepage: www.journals.elsevier.com/spectrochimica-acta-part-a-molecular-and-biomolecular-spectroscopy

MOF-integrated fluorescent composites and adsorbents for rapid detection and removal of date-rape drugs

Kornelia Hyjek [a], Grzegorz Kurowski [a], Anna Pajdak [b], Łukasz Kuterasiński [c], Sylwia Tomczyk [a], Klaudia Jasińska [a], Patryk Szymaszek [a], Joanna Ortyl [a], Piotr Jeleń [d], Maciej Sitarz [d], Witold Piskorz [e], Przemysław J. Jodłowski [a,*]

[a] Cracow University of Technology, Faculty of Chemical Engineering and Technology, Warszawska 24, PL-31-155, Kraków, Poland
[b] Strata Mechanics Research Institute, Polish Academy of Sciences, Reymonta 27, PL-30-059, Kraków, Poland
[c] Jerzy Haber Institute of Catalysis and Surface Chemistry, Polish Academy of Sciences, Niezapominajek 8, PL-30-239, Kraków, Poland
[d] Faculty of Materials Science and Ceramics, AGH University of Krakow, Mickiewicza 30, PL-30-059, Kraków, Poland
[e] Faculty of Chemistry, Jagiellonian University in Kraków, Gronostajowa 2, PL-30-387, Kraków, Poland

HIGHLIGHTS

- γ-hydroxybutyric acid detector based on proflavine@metal–organic framework is shown.
- PF@MOF fluorescent composites designed for rapid identification of GHB-Na.
- Selective absorption shift observed exclusively in presence of GHB-Na.
- UiO-66-based MOFs exhibit high GHB-Na uptake up to 3000 mg g^{-1} in alcoholic media

GRAPHICAL ABSTRACT

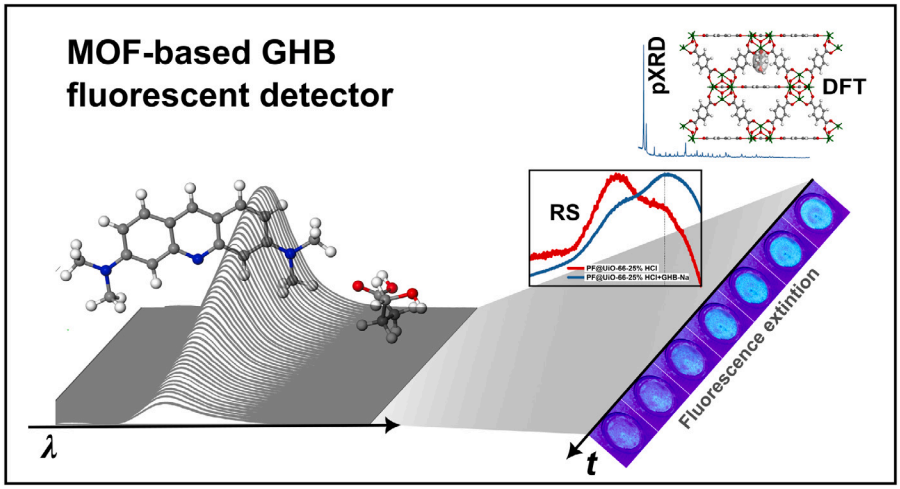

ARTICLE INFO

Keywords:
Proflavine
Metal–organic frameworks (MOF)
Fluorescent composites
γ-hydroxybutyric acid (GHB) detection
DFT calculations

ABSTRACT

In this study, a series of fluorescent composites based on the proflavine@metal–organic framework (PF@MOF) for the detection of a common "date-rape drug" was designed and complementarily characterized. The luminescence efficiency was examined in a γ-hydroxybutyric acid (GHB)/ethanol (EtOH)/acetone (Ace) series upon irradiation with 455 nm light. The characteristic green luminescence was noticeable for mixtures containing GHB-Na, and the luminescent effect lasted up to 5 min for the concentrations as low as 6 mg mL^{-1}. Additionally, to comprehensively characterize the obtained PF@MOF materials, the luminescence kinetics experiments were performed, which showed the persistence of the effect after 4 min of analysis. A significant

* Corresponding author.
E-mail addresses: kornelia.hyjek@doktorant.pk.edu.pl (K. Hyjek), grzegorz.kurowski@pk.edu.pl (G. Kurowski), pajdak@imgpan.pl (A. Pajdak), lukasz.kuterasinski@ikifp.edu.pl (Ł. Kuterasiński), wpiskorz@chemia.uj.edu.pl (W. Piskorz), przemyslaw.jodlowski@pk.edu.pl (P.J. Jodłowski).

https://doi.org/10.1016/j.saa.2025.127375
Received 9 September 2025; Received in revised form 19 November 2025; Accepted 20 December 2025
Available online 22 December 2025

shift in the absorption maximum and an increase in intensity were found after adding the GHB-Na/EtOH/Ace mixture. The wavelength shift occurs only in the presence of GHB-Na, proving the high selectivity of the developed composites. To comprehensively understand the detection mechanisms, the developed materials were characterized by several characterization and computational methods, including powder X-ray diffraction (PXRD), Raman spectroscopy, Diffuse Reflectance IR Spectroscopy (DRIFTS), low-temperature N_2 sorption, Density Functional Theory (DFT) modeling, and Scanning Electron Microscopy (SEM). Apart from confirmed properties for detecting GHB-Na in alcoholic environments, the parent MOFs have proven to have high GHB-Na adsorption properties. The highest GHB-Na adsorption capacity in water was obtained for defective UiO-66%–25% HCl, reaching 2000 mg g^{-1} MOF, whereas in 20% EtOH solution, 3000 mg g^{-1} GHB-Na removal was obtained for UiO-25% HCl and functionalized UiO-66-SO_3H. The developed composited materials and their parent counterparts have proven high potential as GHB-Na fluorescent detectors and efficient GHB-Na adsorbents. The unprecedented properties of the obtained materials have revealed their great potential for real-world applications, including the prevention of sexual assault with the use of GHB-Na.

1. Introduction

Over the years, drug abuse has become an increasingly serious social problem, posing urgent challenges from both social and public health perspectives. The effects of abused compounds are specific and depend on their chemical structure as well as their target sites in the body. Among many psychoactive substances, 4-methylmethcathinone (mephedrone, 4-MMC), methylenedioxymethamphetamine (MDMA) which produces similar to those of amphetamines [1,2], *D*-lysergic acid diethylamide (LSD) which has hallucinogenic effect [3,4], opioids (morphine, heroin, fentanyl), which posses a sedative impact [5–7], γ-hydroxybutyrate or γ-hydroxybutyric acid (GHB), and the precursor – γ-butyrolactone (GBL), are commonly abused. Some of these drugs are used for criminal purposes, such as sexual assault, rape, or abuse in clubs, and are therefore referred to as "club drugs" or "date-rape drugs" [8], and the best known examples are GHB and GBL.

GHB is typically used to sedate the victim, increase libido, and induce short-term amnesia and orientation problems, which has led to it being referred to as a cheap and easily available "date-rape pill", "liquid ecstasy", or "liquid X" [9–11]. Besides, such properties predestinate GHB also as a pharmaceutical [9] to treat depression and sleep disorders and for voluntary, recreational purposes.

As an illegal drug used in a sexual context, it is very often dissolved in water or alcoholic beverages in clubs. The different effects of GHB are related to the dose administered. Light doses of 0.5–1 g are used recreationally, inducing euphoria. Doses in the 2.25–4 g range cause loss of consciousness and are administered in sexual assaults [10,12]. Therefore, there is a strong demand for the development of its quick and simple detection methods. Due to its small molecular weight and simple chemical structure, GHB remains difficult to identify. Currently, many methods of identification of this party drug are known and described in the literature [10,11,13–22]. Most methods are based on instrumental analytical methods using professional equipment such as gas chromatography-tandem with mass spectrometry (GC–MS/MS) [17,18,23–25], high-performance liquid chromatography combined with mass spectrometry (HPLC-MS/MS) [3,10,22,26,27], ion exchange chromatography (IC) [18], Total Vaporization Solid-Phase Microextraction (TV-SPME) [27], or nuclear magnetic resonance spectroscopy (NMR) [11]. Therefore, it is evident that these techniques cannot be applied for rapid, on-site detection of GHB.

In the work by Elie et al. [21], an innovative method was proposed using microscope glass plates with $La(NO_3)_3$:$AgNO_3$, where the presence of GHB induces the formation of "GHB right-angle crystals".

Another way of GHB detection was the development of nail polish, which changes color when the compound is present. The nail polish has been shown to detect GHB, but its effectiveness has not yet been confirmed in complex alcoholic beverage matrices [28]. The so-called "second skin", although potentially suitable for practical use in everyday situations, is still in the early stages of testing. Despite several publications and studies on GHB detection to the "naked eye", several gaps remain, showing that there is a lack of rapid, simple, inexpensive, and effective methods for GHB detection in everyday life situations.

Among a diverse group of materials, metal–organic frameworks (MOFs) have attracted growing attention from the scientific community. These structures consist of metal centers coordinated to organic linkers, forming highly porous frameworks with well-defined architecture. Features such as high chemical and thermal stability, large specific surface areas, low toxicity, or high biocompatibility make MOF suitable for a wide range of applications, from catalysis to medical applications [29–39] .

In our previous studies, we proposed the use of zirconium-based MOFs as novel materials for drug detoxification during the acute overdose [40,41]. The developed detoxification systems may act simultaneously as efficient drug adsorbents [41] and antidote carriers [42], thereby acting as a drug antagonist at the same time. Moreover, MOFs have also been used as adsorbents for a variety of drugs and have found applications in water purification processes [43–46].

Apart from the use of MOF as drug adsorbents or cargos, MOF-based fluorescent detectors have been reported as having great potential in the detection of environmental pollutants and hazardous pharmaceutical drugs [47]. By varying MOF properties such as metal type, linkers, and the presence of guest molecules, they can exhibit fluorescence, making them promising luminescent materials. The primary sources of luminescence in MOFs are the metal nodes, organic linkers, metal–ligand charge transfer, and the incorporation of guest particles within their pores. These unique MOF properties, together with a high possibility of MOF modification at synthesis and post-synthesis stages, allow for the development of sensing materials designed for the detection of specific analytes.

Thus, in this manuscript, we present a novel GHB detection system based on MOFs functionalized with proflavine (PF) fluorescent dye (PF@MOF) as an efficient and fast detector of GHB in alcoholic beverages. The presented research includes a description of the synthesis of the materials, the incorporation of the PF dye as a fluorescent sensor for detection, the process of GHB sorption on parent MOF materials, and complementary physicochemical characterization of the obtained MOFs, PF@MOFs, and composites after drug sorption, GHB@MOFs. In addition, visual detection tests of GHB with PF@MOFs in a variety of media, including alcoholic beverages, kinetics measurements of GHB on PF@MOFs, and spectrofluorometric measurements were performed. The developed composite materials offer a novel approach for detecting GHB in beverages using MOFs functionalized with a fluorescent PF probe.

2. Experimental

2.1. Material synthesis and characterization

In this article, a series of Zr-based MOFs were synthesized and characterized, including UiO-66 obtained in modulated synthesis with hydrochloric acid, denoted as UiO-66-25%HCl [42,48,49], and functionalized with a sulfonic group -SO_3H and referred to as UiO-66-SO_3H [50,51]. The third of the materials used was MOF-808 [42,

52]. The UiO-66-25%HCl, UiO-66-SO_3H, and MOF-808 were synthesized by solvothermal methods following the procedures described elsewhere [42,48,51]. The detailed synthesis procedures and activation methods of the parent MOF are described in the Supporting Information. The obtained MOFs were fractionated, and the fraction with particle size in the 0.05–0.1 mm range was used in all studies. The obtained materials were characterized by a series of physicochemical studies, including X-ray diffractometry (PXRD), diffuse reflectance infrared Fourier transform spectroscopy (DRIFTS), μRaman spectroscopy, scanning electron microscopy (SEM), and low-temperature adsorption N_2. A detailed description of characterization methods is provided in the Supporting Information.

2.2. Proflavine@MOFs (PF@MOFs) composites as GHB detect agents

To obtain a MOF-based fluorescent composite for the efficient detection of GHB in alcoholic beverages, pristine MOFs were loaded with a fluorescent dye, proflavine (PF). The composite PF@MOF materials were obtained by weighing 300 mg of MOFs (UiO-66-25%HCl, UiO-66-SO_3H, and MOF-808) and 5 mg of PF, which was dissolved in 10 mL of acetone. Subsequently, MOF was placed in the resulting dye solution, put on a magnetic stirrer, and stirred for 2 h at room temperature. After this time, the resulting PF@MOF composites were centrifuged at 6000 rpm for 10 min. The resulting precipitate was our composite material PF@MOFs, specifically, PF@UiO-66-25%HCl, PF@UiO-66-SO_3H, and PF@MOF-808. The resulting filtrate was used to determine the degree of PF loading in the MOF. For this purpose, the UV–Vis spectrum of the solution was measured. The amount of dye, C (mg mL^{-1}), was determined from a previously prepared calibration curve of PF in acetone using the same spectrophotometer. The following formula was used to calculate the actual amount of dye loaded into the MOF structure [39]:

$$\text{Proflavine(wt.\%)} = \left[\frac{m_{PF} - C \cdot V}{m_{MOF} + m_{PF} - C \cdot V}\right] \cdot 100, \quad (1)$$

where: m_{PF} – PF amount used to prepare PF acetone solution for PF loading procedure, 5 mg,

m_{MOF} – MOF mass used for preparation of PF@MOF composite, 300 mg,

C – Proflavine concentration in the filtrate (mg mL^{-1}),

V – volume of the solution, 10 mL.

2.3. Spectrofluorometric measurement

The spectrofluorometric measurement involved two experiments and was carried out for the following materials: pristine MOFs, PF dye, and PF@MOF composites. The first experiment consisted of exposing the respective material to light at a wavelength of 580 nm to obtain the sample's excitation spectra and to determine the wavelength at which it reaches a maximum. The excitation spectra were collected in the range of 300–550 nm. The second measurement focused on examining the material's emission spectra. Consequently, the sample was exposed to light at the wavelength at which excitation spectra reach a maximum, i.e., 455 nm, and the spectrum was collected in the range of 470–800 nm. The changes in wavelength and intensity in the emission and excitation of the sample under the addition of the following solvents were checked: EtOH, Ace, 48 mM GHB-Na sodium solution, a mixture of ethanol with GHB-Na solution, a mixture of acetone with GHB-Na solution, and a mixture of ethanol, acetone, and GHB-Na solution. Fig. 1 illustrates a summary of the materials and solvents used, along with the emission and excitation intensities of the samples.

The sample matrix presented in Fig. 1 allowed for the determination of the most efficient and selective GHB-Na detectors under various conditions. The selectivity of the materials was evaluated. The measurement was intended to illustrate the differences between the emission and excitation spectra of PF@MOFs composite materials under the influence of the addition of GHB-Na. Such an experiment highlighted the possibilities of GHB-Na detection using spectrofluorimetric techniques. Details of the type and parameters of the instrument are provided in the Supporting Information file. The spectrofluorimetric measurements procedure was based on measuring the spectrofluorimetric spectra by subsequently adding dropwise reagents according to the sample matrix (Fig. 1), i.e., 2.5 μL of a 48 mM GHB-Na solution and/or 5 μL of EtOH/Ace/EtOH+Ace solution to the 5 mg of material with a size fraction of 0.05–0.1 mm particles. The maximum excitation was observed at 455 nm.

2.4. Kinetics of luminescence for composites PF@MOFs study

A series of experiments on luminescence kinetics was conducted to determine the kinetics of luminescence and, thus, the rate of luminescence extinction in prepared PF@MOF composites. In brief, 5 mg of each PF@MOF (PF@UiO-66-25%HCl, PF@UiO-66-SO_3H, and PF@MOF-808) was weighed, then 5 μL of EtOH was added, and the measurement was performed. The operation was repeated, after adding 2.5 μL of GHB-Na (48 mM) and 5 μL of EtOH sequentially, and for 2.5 μL of GHB-Na (48 mM), 5 μL of EtOH, and 5 μL of Ace. The spectra were collected over approximately 4 min and at a wavelength of 365 nm.

2.5. Spectrofluorometric measurement of actual samples

The practical feasibility of prepared materials was tested via spectroscopic measurements on actual samples. The detailed list of beverages tested in this study is presented in the Supporting Information file (Table S1). In this experiment, eight model beverages were tested using the spectroscopic method described above (cf. Spectrofluorimetric measurements subsection), with the difference that 2.5 μL of GHB-Na (48 mM) and 5 μL of Ace were added to the 5 μL of alcoholic beverage.

2.6. "Naked eye" GHB-Na detection

To demonstrate the possibility of detecting GHB-Na with the obtained PF@MOFs composite materials without instrumental methods, the following experiments were performed: 20 mg of each composite material PF@MOFs with a size fraction of 0.05–0.1 mm particles were weighed, and the sample was placed in a rubber ring in a dark chamber in the presence of the 455 nm wavelength light of a 900 mW LED. A 48 mM GHB-Na solution of 10 μL and/or 20 μL of EtOH/Ace/EtOH+Ace solvent was added next, analogously to the spectrofluorometric experiment mentioned above and according to the heatmap shown in Fig. 1. From the moment the specific solvent was spotted, the time was measured, and the luminescence, or lack of it, in the material was observed. Photographs were taken by NIKON D3300 camera at intervals depending on the sample type and related to the extinction of the material's luminescence. The maximum measurement duration was 5 min. The illumination was observed with the "naked eye", and the camera was used to catch the shot and provide evidence of the execution of the experiment.

2.7. GHB-Na sorption process

To study the adsorption efficiency on prepared materials, the adsorption tests were performed on previously activated UiO-66-25%HCl, UiO-66-SO_3H, and MOF-808 samples, respectively. In adsorption experiments, 25 mg of MOF was weighed after activation and placed in plastic cups, and 15 mL of a 48 mM GHB-Na aqueous solution was added. Three separate sorption tests were performed for each adsorption experiment. The measurement was performed under thermostatic conditions at 25 °C. Samples of 0.5 mL were taken at specific time intervals: 5 min, 15 min, 30 min, 45 min, 1 h, 2 h, 4 h, 6 h, and 24 h. Each sample was filtered through a 45 μm diameter nylon

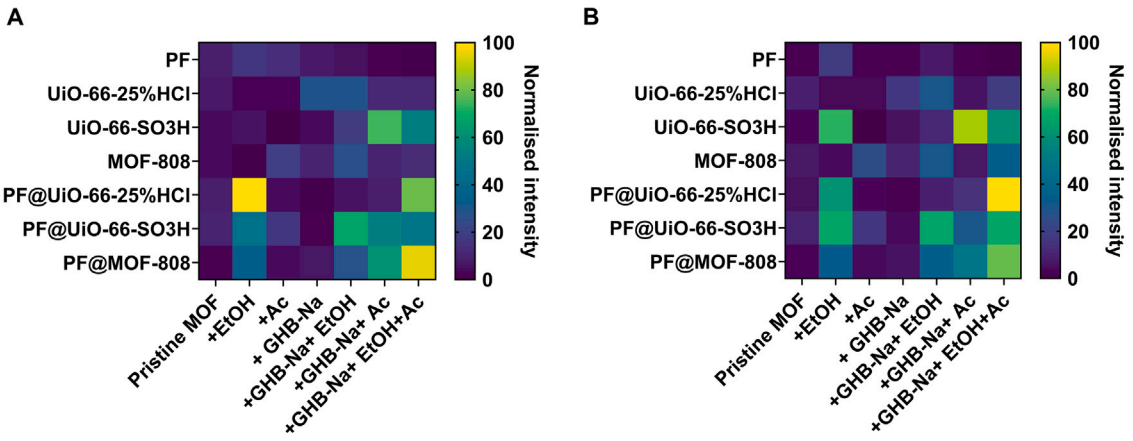

Fig. 1. Heatmap and correlation matrix during the spectrofluorimetric experiments; (**A**) excitation spectra collected at the range 300–550 nm (at λ_{max-em} = 580 nm); (**B**) emission spectra measurement at 470–800 nm (at λ_{max-ex} = 455 nm); **PF** – proflavine, **EtOH** – ethanol, **Ace** – acetone.

syringe filter and then analyzed using high-performance liquid chromatography (HPLC). The specifications of the instrument, along with the methodology for measuring GHB-Na concentrations, are described in the Supporting Information file. After the sorption process, the solutions were centrifuged at 6000 rpm for 10 min. The obtained precipitates were composite materials with GHB loaded into the MOF structure, denoted as GHB@MOFs.

2.8. Computational simulations

The density functional theory (DFT) simulations utilized the VASP code, and the initial structures were derived from classical forcefield-based Monte Carlo (MC) simulations. The DFT simulations allowed for the geometry optimization of the GHB-Na molecule in four locations obtained via MC. The computational parameters of the optimization methods and atomic charge and bond order simulations are given elsewhere [40–42,53]. Besides the calculations mentioned above, in this article the UV–Vis absorption spectra were simulated with the use of Gaussian code [54] at the TDDFT [55–57] level of theory, with the use of the hybrid B3LYP [58] correlation-exchange functional, LanL2DZ [59,60] basis set, and with solvent PCM [61] approximation.

3. Results

3.1. Synthesis and characterization

In this work, three types of zirconium-based metal–organic frameworks were synthesized and characterized in terms of their applicability for "date-rape drug" detection and removal. Two materials originated from the UiO-66 family, with varying synthesis methods using modulated synthesis with hydrochloric acid, denoted as UiO-66-25%HCl and UiO-66 functionalized with -SO_3H groups and denoted as UiO-66-SO_3H. The third MOF used for GHB detection and adsorption was MOF-808, representing the Zr-based group; however, the ligand forming the MOF framework contains an additional carboxyl group - benzene-1,3,5-tricarboxylic acid (H_3BTC, trimesic acid) than in the case of UiO-66 (H_2BDC, terephthalic acid).

The syntheses for both parent MOFs, PF@MOFs, and GHB@MOFs composites were validated by powder X-ray diffractometry PXRD (Fig. 2, Figure S1). Diffractograms of prepared MOFs [42,62–64], and GHB-Na [20] are widely described and available in the literature [20, 42,62–64]. The comparison of the obtained results with those taken from the literature confirms the high crystallinity of the prepared materials. In addition, PXRD results for PF@MOF composites have proven the high crystallinity of the prepared materials after the introduction of PF fluorescent dye. Additionally, the stability and crystalline character of the MOF frameworks were also preserved after the GHB-Na sorption process for GHB@UiO-66-25%HCl and GHB@UiO-66-SO_3H.

However, the diffractogram of GHB@MOF-808 shows a slight loss of stability of MOF-808 after the GHB-Na adsorption process. This is visible as a change in the intensity of the reflections and may be due to partial degradation and collapse of the material after 24 h of the sorption process.

The porous structure of prepared materials was determined by the low-temperature adsorption of nitrogen (Fig. 2B, C, Table 1).

The N_2 adsorption isotherms of UiO-66-25%HCl and MOF-808 were determined as type I according to IUPAC [65]. In UiO-66-SO_3H, a type III isotherm was found for both the pristine material and after the PF sorption. Theoretical models were used for N_2 adsorption points as a function of pressure $0 < p/p0 < 0.996$, and the parameters of the pore surface structure were determined (Table 1). The highest values were obtained here for the pristine UiO-66-25%HCl and MOF-808 samples. In UiO-66-25%HCl, the multilayer (BET model) and monolayer (Langmuir model) surface areas were 1057 $m^2\ g^{-1}$ and 1709 $m^2\ g^{-1}$, respectively, which is consistent with the literature [42]. The use of hydrochloric acid during the UiO-66 synthesis increased the available pore space of the sample, and the total pore volume (DFT model) of 0.682 $cm^3\ g^{-1}$ was obtained. In pristine MOF-808, the S_{BET} and S_L surface areas were 1130 $m^2\ g^{-1}$ and 1836 $m^2\ g^{-1}$, respectively, and the pore volume was 0.615 $cm^3\ g^{-1}$, which is also consistent with the literature data [42,66]. During the PF adsorption process in both MOFs, the initially open pore space was intensively filled by the PF dye. The BET-specific surface area value in PF@UiO-66-25%HCl decreased to 432 $m^2\ g^{-1}$, while the volume of pores decreased to 0.217 $cm^3\ g^{-1}$. Similarly, in PF@MOF-808, much lower parameter values were obtained compared to pristine MOF-808. The specific surface area parameter value and the shape of the sorption isotherm for pristine UiO-66-SO_3H indicate a predominant share of mesopores in its pore structure. Here, S_{BET} was determined to be 198 $m^2\ g^{-1}$ and V_{DFT} = 0.150 $cm^3\ g^{-1}$, which is in agreement with the literature [67,68]. The PF dye, a relatively large molecule compared to GHB-Na, partially filled the open pores and reduced the pore size.

The pore size distribution (PSD) was determined based on the DFT model (Fig. 2C). A bipolar pore distribution was measured in UiO-66-25%HCl. The pores with the largest volume had diameters of 0.5–1 nm, while the second peak, indicating an increased volume, was in the 1.3–1.7 nm pore range. After PF sorption, the pore volume in both ranges decreased. In MOF-808, the largest volume, measured in the pores, was in the range of 1.5–2 nm and 0.5–0.8 nm. Here, too, PF sorption decreased the open pore volume, although the PSD shape was similar. In pristine UiO-66-SO_3H, pores with a diameter of 1.2–1.8 nm predominated in the structure, which was partially clogged with dye molecules after the sorption process [65].

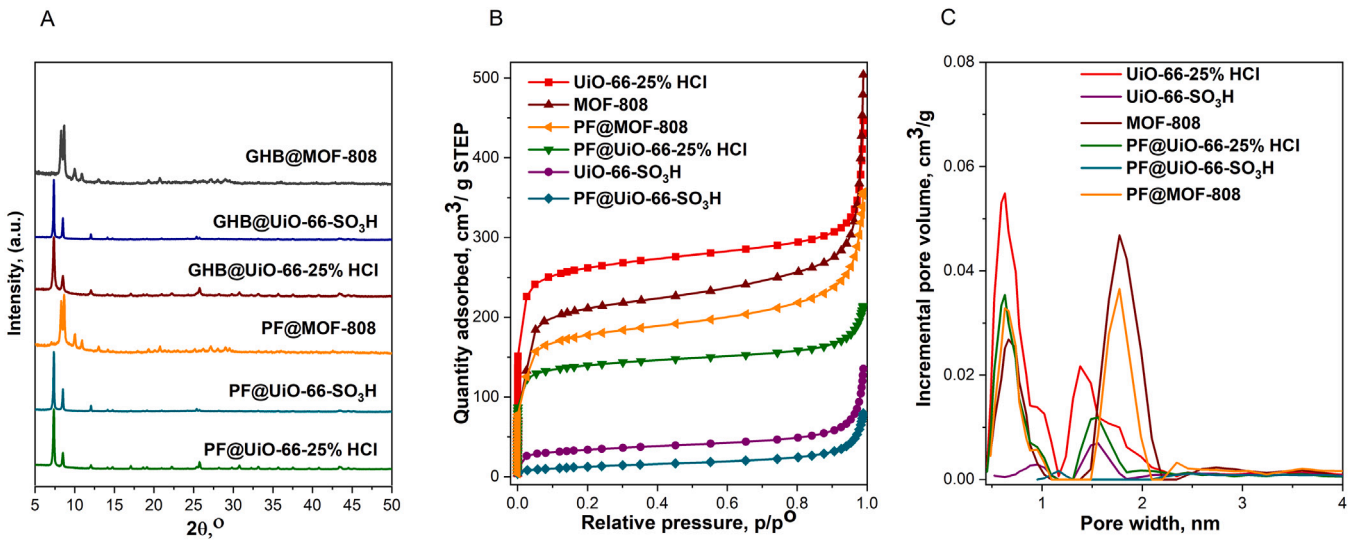

Fig. 2. (**A**) PXRD diffractograms; (**B**) N_2 adsorption isotherms; (**C**) pore size distributions (DFT model). The analysis was performed for pristine MOFs and PF@MOF composites.

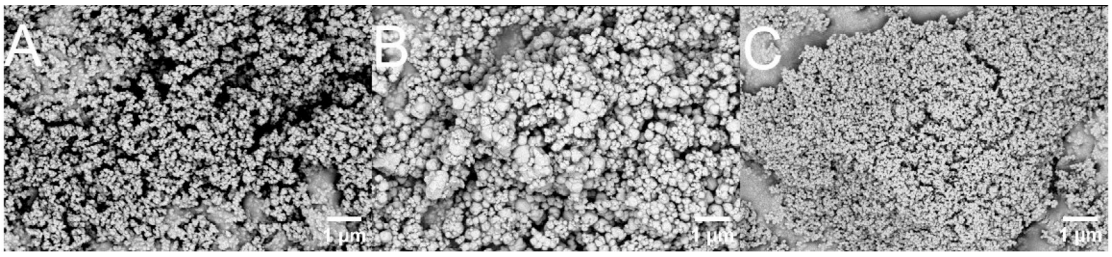

Fig. 3. Figure 3 SEM images for (**A**) PF@UiO-66-25%HCl; (**B**)PF@UiO-66-SO_3H; (**C**) PF@MOF-808.

Table 1
Sample characterization details. $\mathbf{A_m}$ - sorption capacity at 0.1 MPa; $\mathbf{S_{BET}}$, $\mathbf{S_L}$ - surface area according to BET and Langmuir model, respectively; $\mathbf{V_{DFT}}$ - total pore volume according to DFT model.

Sample	PF loading (wt.%)	A_m (cm^3 g^{-1} STP)	S_{BET} (m^2 g^{-1})	S_L (m^2 g^{-1})	V_{DFT} (cm^3 g^{-1})
UiO-66-25%HCl	4.02	602	1057	1709	0.682
(PF@UiO-66-25%HCl)		(214)	(432)	(678)	(0.217)
UiO-66-SO_3H	4.04	244	198	366	0.150
(PF@UiO-66-SO_3H)		(79)	(45)	(103)	(0.017)
MOF-808	4.60	860	1130	1836	0.615
(PF@MOF-808)		(357)	(558)	(912)	(0.342)

To determine the amount of PF adsorbed on prepared MOFs, UV–Vis experiments were performed (Fig. 1) and calculated by using Eq. (1). It may be inferred that the amount of PF adsorbed by MOF samples varies around ca. 4 wt% for PF@UiO-66-25%HCl and PF@UiO-66-SO_3H, whereas for PF@MOF-808 is slightly higher and equal to 4.60 wt%. When comparing the obtained results for PF to those presented in the literature, e.g., propranolol [42], it may be concluded that the PF may be preferably located at the surface of MOF rather than adsorbed inside the pores of MOF.

To characterize the morphology of prepared samples, the microphotographs of prepared PF@MOF samples and parent MOF samples were taken by scanning electron microscopy (SEM, Fig. 3, Figure S2).

It may be observed that the addition of the modulator during the synthesis of UiO-66-25%HCl affected both the size and shape of the crystals, as detailed in the literature [48,69,70], emphasizing the nanometer crystal sizes of UiO-66-25%HCl, as shown in Figure S2 A. The SEM images for UiO-66-SO_3H (Figure S2B) are significantly different from the UiO-66-25%HCl. The obtained crystals possess well-defined round shapes of considerably increased sizes (Figure S2B). For MOF-808, cubic shapes with grain sizes similar to UiO-66-25%HCl were observed, as shown in Figure S2C. No significant differences were observed when comparing the SEM images of pristine MOFs to those obtained for PF@MOF composites. The shape and size of the remaining PF@MOF composites were well preserved in most considered cases except PF@UiO-66-SO_3H, where a slight increase in the crystal size was observed (cf., Fig. 3B and Figure S2B).

To comprehensively characterize the molecular nature of the prepared materials, DRIFTS and μRaman spectroscopy were performed. The DRIFT spectroscopy results are presented in Fig. 4.

The DRIFT spectra for pristine MOFs are in good agreement with the data widely available in the literature [41,42,70–72] (Fig. 4). The bands in the range of 3500–2500 cm^{-1}, especially visible in the UiO-66-SO_3H spectrum, originate from the -OH groups, most likely air moisture [72]. The band at a wavenumber of about 1600 cm^{-1} is associated

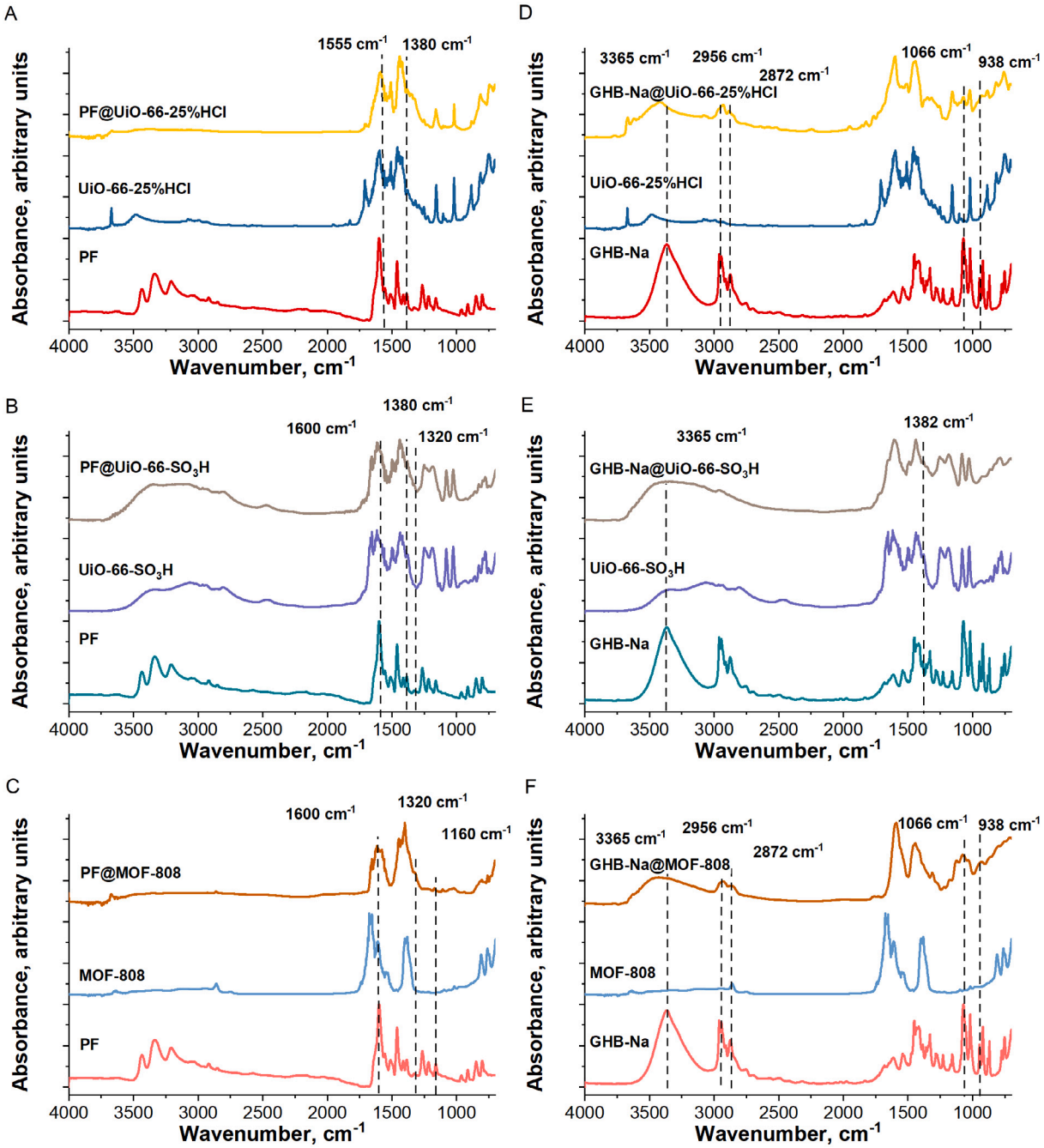

Fig. 4. FTIR spectra of pristine MOFs and prepared composites PF@MOF and GHB@MOF. (**A**, **D**) UiO-66-25%HCl; (**B**, **E**) UiO-66-SO_3H; (**C**, **F**) MOF-808. Spectra of MOFs and composites by DRIFT and spectra of PF by ATR-FTIR.

with a carboxyl group, more precisely with the C–C bond of an aromatic compound forming the organic linker of the MOF network [72]. Similarly, the band at 1385 cm^{-1} corresponds to C-O stretching vibrations in the C-O group [72]. The band at 745 cm^{-1}, found on all spectra of pristine MOFs, confirms the presence of Zr-O nodes [50,51]. The band between 1750 cm^{-1} and 1000 cm^{-1} corresponds to C=C stretching vibrations [72,73]. In addition, the UiO-66-SO_3H spectrum shows an additional band at 1085 cm^{-1} corresponding to the S-O stretching vibration [74,75]. Similarly, a band at 1245 cm^{-1} is associated with the O-S-O bond [74,75]. Bands characteristic for the pristine PF dye were visible at 1600 cm^{-1}, 1510 cm^{-1}, and 1320 cm^{-1}, and were associated with C=C stretching vibrations [76,77]. Moreover, the band at 1555 cm^{-1} corresponds to C-N stretching vibrations [77]. The band at 1160 cm^{-1} is responsible for C-H bending vibrations [77]. The bands at 1380 cm^{-1} and 1322 cm^{-1} are associated with N-H bending vibrations. The spectrum of pristine GHB-Na shows characteristic bands at wave numbers 938 cm^{-1} and 1010 cm^{-1} originating from C–C vibrations [78,79]. The band at 1066 cm^{-1} is associated with C-O stretching vibrations [80]. In addition, a weak band visible at 1382 cm^{-1} corresponds to the wagging band -CH_2-. For the sodium salt of GHB-Na (Fig. 4D, E, F), characteristic bands are also present at 1531 cm^{-1} and 1415 cm^{-1} and are associated with the carboxyl group [81]. A band at 1680 cm^{-1} associated with the OH group is also clearly visible [78,80]. High intensities of bands at 3365 cm^{-1}, 2950 cm^{-1}, and about 2872 cm^{-1}, correspond to stretching O-H and stretching CH_2 vibrations [80], respectively. On the spectra of GHB-Na@UiO-66-25%HCl (Fig. 4D) and GHB-Na@MOF-808 (Fig. 4F) composites, the

bands from the drug are visible, highlighting the efficiency of GHB-Na sorption over MOFs. In both cases, the presence of GHB can be confirmed by bands such as 938 cm^{-1}, 1066 cm^{-1}, and – the most intense – 2872 cm^{-1}, 2956 cm^{-1}, and 3365 cm^{-1}. On the spectrum of the GHB-Na@UiO-66-SO_3H (Fig. 4E) composite, only two bands can be identified at 938 cm^{-1} and 3365 cm^{-1}. In the other cases, the bands are not visible or are hidden by bands associated with the MOF structure. However, this does not undermine the material sorption capacity, as confirmed by other techniques, described later in the article.

The μRaman spectroscopy analysis results for GHB-Na, parent MOF samples, PF@MOF prepared composite samples, and PF@MOF composite samples upon GHB-Na addition are provided in Fig. 5 and Figure S3, respectively. The μRaman spectra for pristine MOF materials agree well with our previous results and are described in detail elsewhere [40–42, 82]. The μRaman spectra of PF (Fig. 5, Figure S3) reveal characteristic bands in the region of 1500–1000 cm^{-1}, with the most visible band at 1414 cm^{-1}, which are characteristic of C–C in-plane stretching and C–C-C bending [83]. The PF characteristic band at 1414 cm^{-1} was detected for all PF@MOF composite samples (Fig. 5A-C), observed as a considerable band intensity increase when compared with pristine MOF samples (Figure S3). The GHB-Na μRaman spectrum is presented in Fig. 5A-C. The characteristic bands at 1430 cm^{-1}, 1295 cm^{-1}, 923 cm^{-1}, and 486 cm^{-1} are associated with CH_2 bending, CH_2 waging, CH_2 rocking, and CO_2 rocking, respectively. It must be pointed out that when adsorbing GHB-Na over prepared PF@MOF samples, the characteristic bands are weakly visible due to the overlap of the PF and MOF characteristic bands. However, in the case of PF@UiO-66-25%HCl+GHB-Na, when using a 785 nm laser line, a subtle band shoulder increase may be observed (Fig. 5A). However, an interesting observation was made when using a laser with a 488 nm line (Fig. 5D-F). In all considered composite PF@MOF samples, sizable fluorescence was observed with the maximum at 1890 cm^{-1}; however, upon the addition of GHB-Na, the band shifts towards 885 cm^{-1}. The most considerable shift was observed for PF@UiO-66-25%HCl and PF@UiO-66-SO_3H samples (Fig. 5D, E), respectively. Apart from the significant shift, the spectacular fluorescence was noticed in both μRaman and visual observations.

3.2. Spectrofluorometric measurements and DFT simulations

This study scrutinizes the applicability of fluorescent PF@MOF probes for detecting sodium γ-hydroxybutyrate (GHB-Na) using spectrofluorometric analysis. The emission and excitation spectra, particularly the variations in band appearance and shifts in the wavelength of maximum intensity, confirm the potential of these probes for detecting illicit substances such as “date rape” drugs.

Before the spectrofluorimetric measurements, DFT simulations were performed to determine the vibronic spectra of PF and GHB-PF adducts. The vibronic spectra of PF in vacuum and in a polarizable environment (water) are presented in Figure S4. The GHB-PF structures were optimized at the DFT level of theory (B3LYP functional), then reoptimized at the TD-DFT level with the same correlation-functional and basis set. The obtained geometries are presented in Figures S5-S8. The TDDFT UV–Vis modeled vibronic spectra for the PF molecule and the PF-GHB adduct are presented in Figures S9-S11. It can be seen that the introduction of the solvent increases the transition moments, induces the appearance of the band at ca. 315 nm, and red-shifts the band at ca. 420 nm to 465 nm and the band at ca. 495 nm to 510 nm. The differences in spectra of structures 1 and 2 are negligible.

For the emission spectrum of the PF dye, excitation at 455 nm results in a maximum emission at 560 nm in the absence of solvents. Upon adding EtOH, Ace, and GHB-Na, however, the emission band shifts to 522 nm, as depicted in Figure S12H (Supporting Information). Similarly, in the excitation spectrum recorded at 580 nm, the maximum is observed at 455 nm for pure PF. These spectral characteristics align with emission and excitation profiles for PF in liquid form previously reported [84–86].

The emission spectra of pristine MOFs exhibit differences compared to those of pure dye; however, no significant spectral variations were observed for UiO-66-25%HCl, UiO-66-SO_3H, and MOF-808. In all considered materials, the maximum emission occurs at 502 nm, regardless of whether pristine MOFs or MOFs with solvents are analyzed. In contrast, the excitation spectrum shows a maximum at 455 nm for pristine MOFs and does not change significantly after adding solvents (Figure S12-A-F). These findings demonstrate distinct spectral behavior between PFs and MOFs and also confirm that solvent addition does not influence the emission and excitation properties of pristine MOFs.

When examining the composite PF@MOF probes, distinct trends emerge. For PF@UiO-66-25%HCl, the maximum emission occurs at 515 nm. Adding EtOH or Ace induces a slight shift towards lower wavelengths, while the presence of GHB – alone or in combination with EtOH and Ace – causes a minor shift towards higher wavelengths. Specifically, the emission maximum shifts from 515 nm to 510 nm, accompanied by a significant broadening of the emission band, particularly in the presence of GHB and the solvent mixture (EtOH and Ace), as illustrated in Fig. 6A, B.

A comparable trend was observed for the PF@UiO-66-SO_3H composite. In its pristine form, the emission maximum occurs at 512 nm, similar to that of PF@UiO-66-25%HCl. However, adding GHB/EtOH/Ace results in a shift to 506 nm (Fig. 6C, D), though without pronounced band broadening. In contrast, PF@MOF-808 exhibits a maximum emission at 510 nm, which increases to 513 nm upon exposure to GHB/EtOH/Ace, as shown in Figures 6E, F. Although the shift is relatively minor, the emission band broadens significantly. Notably, the PF@MOF-808 probe exhibits an increase in emission wavelength in the presence of GHB and solvent mixtures, whereas PF@UiO-66-25%HCl and PF@UiO-66-SO_3H show a decrease in wavelength at the emission maximum.

In each case, detectable changes in the emission spectrum highlight the potential of these probes for assessing the presence of GHB-Na in ethanol-based solutions following acetone addition. However, while acetone is not essential for spectral shifts with PF@UiO-66-25%HCl and PF@UiO-66-SO_3H – since GHB and EtOH alone induce measurable shifts – it is crucial for PF@MOF-808. No significant spectral shift is observed without Ace, even in the presence of GHB and EtOH, emphasizing its necessity for this specific probe.

The exact emission shifts induced by various solvents and solvent-GHB mixtures, as summarized in Fig. 1, are depicted in Fig. 6A-F. These figures also present excitation spectra, which reveal that the excitation maximum in pristine PF@MOF occurs at 455 nm and is not shifted upon addition of the GHB/EtOH/Ace mixture. Consequently, excitation spectra do not provide useful information for GHB detection, as they remain largely similar regardless of whether they are recorded for MOFs or PF@MOF composites.

Overall, GHB detection relies primarily on emission spectra, which demonstrate significant spectral variations. Moreover, the emission spectra of PF dye in the presence of a GHB/EtOH/Ace mixture, pristine MOFs with solvents, and PF@MOF composites exhibit distinct characteristics. These findings underscore the high selectivity of the proposed PF@MOF materials for GHB-Na detection. The observed wavelength shifts and band broadening at the emission maxima serve as clear indicators of GHB-Na presence, confirming the effectiveness of these fluorescent probes for forensic and analytical applications.

To summarize and visualize the spectrofluorimetric measurements, the heatmaps based on the spectra intensities were plotted for the whole matrix of considered samples (Fig. 1). Initially, each sample was irradiated with 580 nm light, and then the excitation of compounds was measured. However, a lack of selectivity towards the GHB-Na molecule was observed. High-intensity fluorescence (visible yellowish fluorescence) occurred even under the addition of solvents such as ethanol, without the addition of the drug, as shown in Fig. 1A. Nevertheless, the maximum of PF dye at 455 nm was observed. In the next step, the samples were exposed to the mentioned wavelength, and the emission

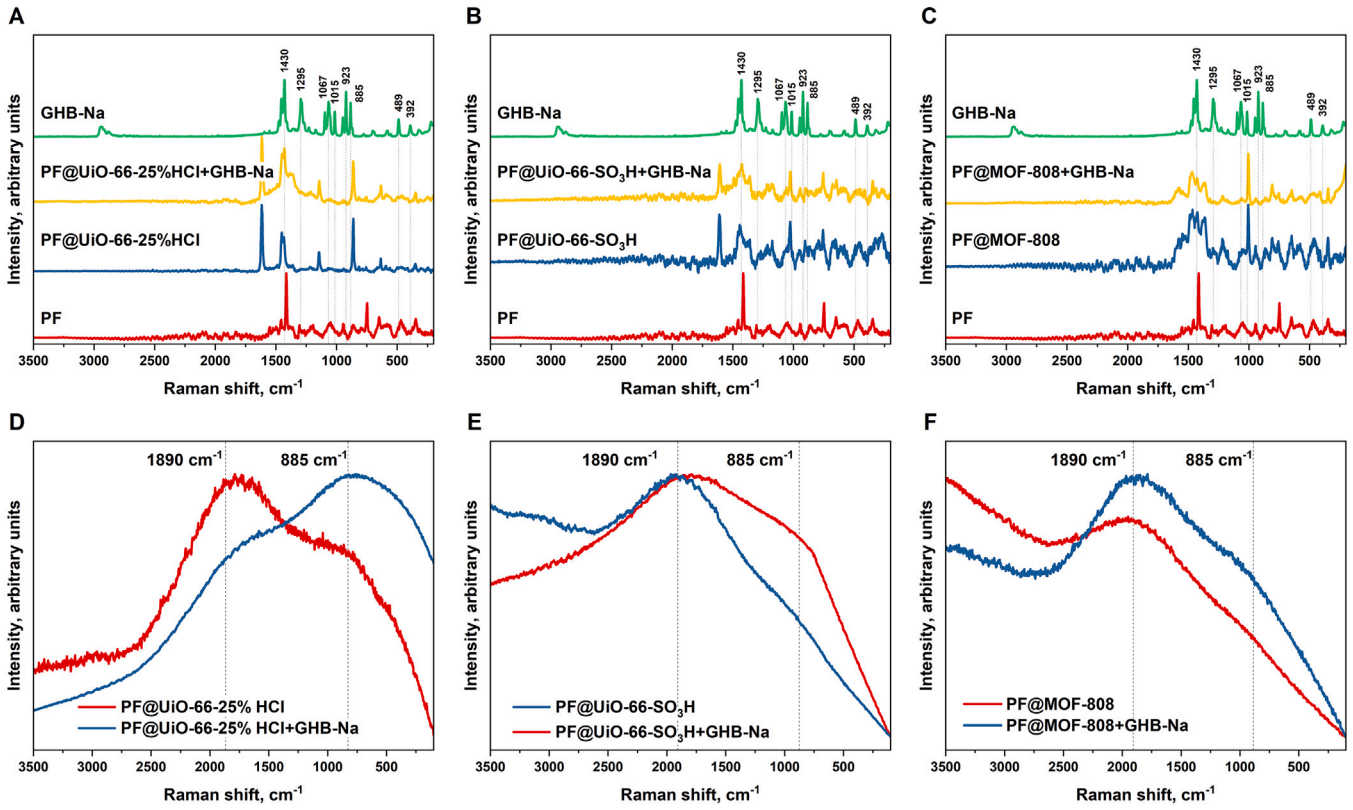

Fig. 5. μRaman spectroscopy results of GHB-Na, PF@MOF prepared composite samples and PF@MOF composite samples upon GHB-Na addition; (**A**-**C**) 785 nm laser line; (**D**-**F**) 488 nm laser line.

spectra were measured. The results showed very high intensities for PF@MOF with the addition of the GHB/EtOH/Ace mixture, of which the PF@MOF composite had the highest selectivity towards GHB-Na (Fig. 1B). The emission and excitation spectra are described in detail above and shown in Fig. 6 and S12. This approach allowed us to select both a suitable analytical method and the most selective probe in the form of PF@MOF for GHB-Na detection.

3.3. Kinetics of luminescence for composites PF@MOFs study

Kinetic measurements provided insights into the luminescence decay rates of fluorescent PF@MOF probes, specifically PF@UiO-66-25%HCl, PF@UiO-66-SO_3H, and PF@MOF-808. The longest and most intense luminescence was observed upon the addition of GHB-Na, EtOH, and Ace, indicating that this solvent mixture, combined with GHB-Na, significantly enhances sample luminescence. This finding suggests the potential applicability of these probes for the detection of illicit substances, such as “date rape” drugs, in forensic and analytical applications.

For PF@UiO-66-25%HCl with the GHB-Na/EtOH/Ace mixture, luminescence kinetics were recorded for 4.15 min, after which a decrease in luminescence intensity and a quenching of the sample were observed. The absorption maximum was detected at 530 nm, with an initial luminescence intensity exceeding 40,000 arb. u., which declined to below 10,000 arb. u. within 4 min. Although a substantial reduction in luminescence was noted, complete extinction did not occur, as illustrated in Fig. 7A. Similarly, the luminescence kinetics of the PF@UiO-66-SO_3H probe (Fig. 7B) were also recorded for 4.15 min. The initial luminescence intensity of approximately 25,000 arb. u. decreased to around 10,000 arb. u. after the set measurement time, representing a comparatively smaller decline in intensity than that observed for PF@UiO-66-25%HCl. The prolonged luminescence of this probe suggests its practical applicability, as it facilitates the observation of the luminescence phenomenon and strengthens the case for its integration into real-world detection systems.

Additional kinetic measurements were performed for PF@MOFs under different conditions: without GHB or solvents, with EtOH alone, and with a combination of GHB and EtOH. The corresponding data are presented in Figure S13 (Supporting Information). The results indicate that PF@MOF composites exhibit intrinsic fluorescence due to the incorporation of the PF dye. The presence of EtOH consistently enhances fluorescence intensity across all tested conditions, whereas the addition of GHB-Na decreases the intensity of fluorescence. Notably, in the absence of Ace, luminescence decay occurs more rapidly for PF@UiO-66-25%HCl. In contrast, for PF@UiO-66-SO_3H, luminescence intensity remains significantly higher after 4 min when compared to samples containing the GHB/EtOH/Ace mixture.

These findings suggest that to achieve complete luminescence extinction, an extended measurement duration would be required. The persistence of luminescence, particularly in certain probe compositions, underscores their potential for practical detection applications and highlights their suitability for monitoring the presence of GHB-Na in forensic investigations.

The PF dye adsorbed on metal–organic frameworks constitutes a fluorophore. Thanks to it, the PF@MOF fluorescent probe exhibits luminescence capabilities under certain conditions. In the case of the experiment in question, the probe is selective and allows detection of the rape pill in the form of GHB. This is related to the mechanism described above for the formation of a hydrogen bond between the negatively charged GHB molecule (after ionization) and the positively charged amino groups in the PF@MOF composite. Although detection is possible in water, the high polarity of H_2O increases the competition for hydrogen bond formation, making luminescence less intense. Therefore, adding ethanol, or acetone with lower polarity, not only increases the intensity of the luminescence but also extends its duration, up to 5 min (Fig. 7). This is due to the lower polarity of both solvents

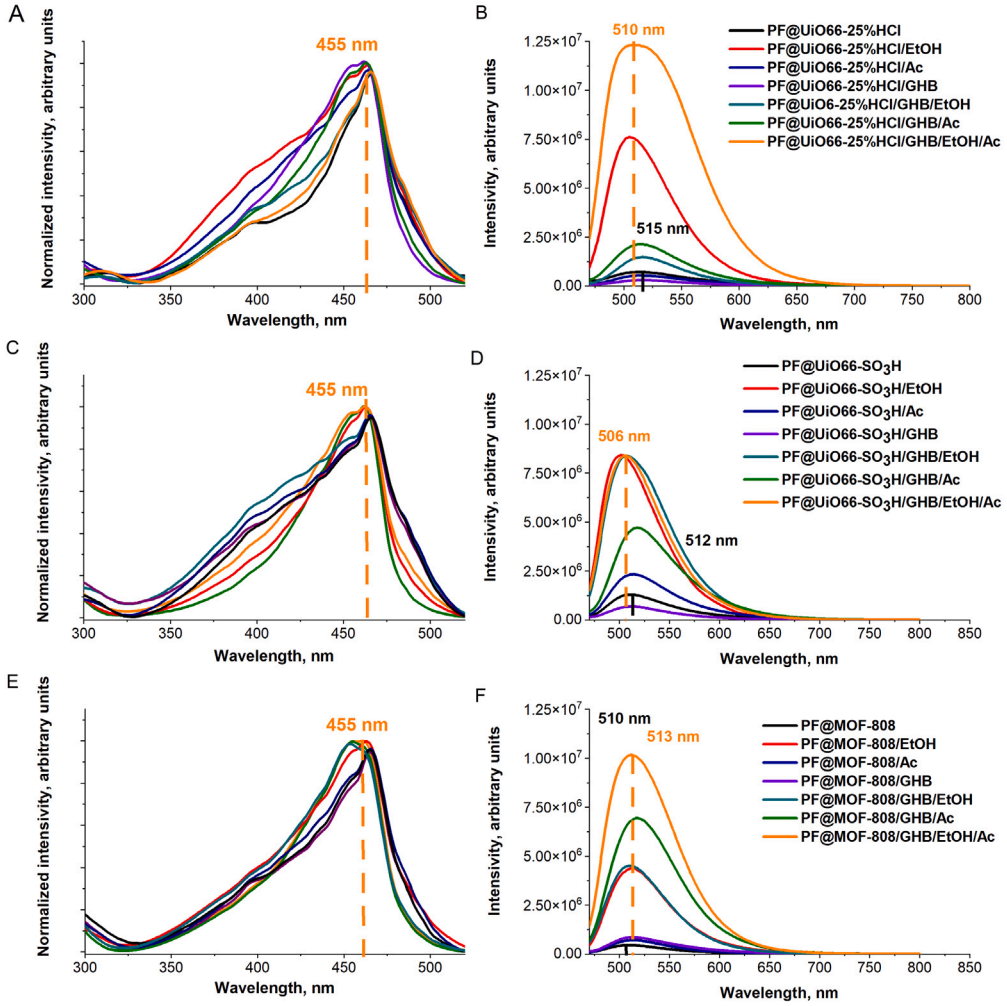

Fig. 6. Spectrofluorometric analysis for prepared PF@MOF composites and solvent additions. Excitation measurement for (**A**) PF@UiO-66-25%HCl; (**C**) PF@UiO-66-SO_3H and (**E**) PF@MOF-808. Emission measurement (**B**) PF@UiO-66-25%HCl; (**D**) PF@UiO-66-SO_3H, and (**F**) PF@MOF-808.

than water, reducing the competition. On the one hand, we observe a visual effect in the form of glowing of the sample with green, intense color, caused by the presence of GHB. On the other hand, however, the resulting hydrogen bonding contributes to a shift in the band of maximum emission intensity, as observed in Fig. 6. The emission in the PF@MOF composite occurs at approximately 515 nm. The addition of GHB, acetone, and ethanol shifts the spectrum by 3–6 nm. This small change makes the probe highly sensitive to the presence of GHB and thus enables the detection of the rape pill. The mechanism of action is the formation of a new hydrogen bond between the PF@MOF composite and GHB. In terms of instrumental analysis, it is observable as a wavelength shift for the sample's emission, and, with the "naked eye", we see a change in the color and luminous intensity of the sample.[87]

3.4. Spectrofluorometric measurement of actual samples

To assess the practical feasibility of the prepared materials on real samples, spectrofluorimetric measurements were performed, and the results are presented in Figure S21. In this experiment, the presence of GHB-Na was tested in eight popular beverages (Table S1). The emission spectra of these beverages without added GHB-Na do not display elevated fluorescence intensity. The average emission intensity for PF@UiO-66-25%HCl, PF@UiO-66-SO_3H, and PF@MOF-808 ranged from approximately 1.25×10^6 to 3.75×10^6 for PF@UiO-66-25%HCl and PF@UiO-66-SO_3H, while the maximum values for PF@MOF-808 were around 6.25×10^6. Upon the addition of GHB-Na to the tested beverages, the fluorescence intensity increased by roughly one order of magnitude compared to the samples without GHB. The most significant luminescence enhancement was observed for PF@UiO-66-SO_3H, where the measured intensity reached up to 1.25×10^7 for six of the eight beverages. Slightly lower increases were recorded for PF@UiO-66-SO_3H/GHB/Drink3/Ac and PF@UiO-66-SO_3H/GHB/Drink1/Ac, with values of 5.00×10^6 and 2.50×10^6, respectively. It is worth noting that although the enhancement in these two cases was not as pronounced as for the other samples, the fluorescence intensity was still significantly higher than that of the reference beverages without added GHB-Na.

3.5. "Naked eye" GHB-Na detection

To confirm the applicability of the designed PF@MOF fluorescent probes in daily applications, the luminescence of the obtained materials upon adding GHB-Na to appropriate solvents was studied. The tests were performed in a dark room in a special chamber with a light-emitting diode at a wavelength of 455 nm. It is also worth mentioning that 455 nm wavelength used for "naked eye" GHB detection is safer for humans than UV light, which was used during the spectrofluorimetric measurements with wavelengths starting at 300 nm.

In this experiment, PF@MOF fluorescent probes PF@UiO-66-25%HCl, PF@UiO-66-SO_3H, and PF@MOF-808, pristine MOFs including UiO-66-25%HCl, UiO-66-SO_3H, MOF-808, and PF dye were examined. This combination was intended to show the specific performance

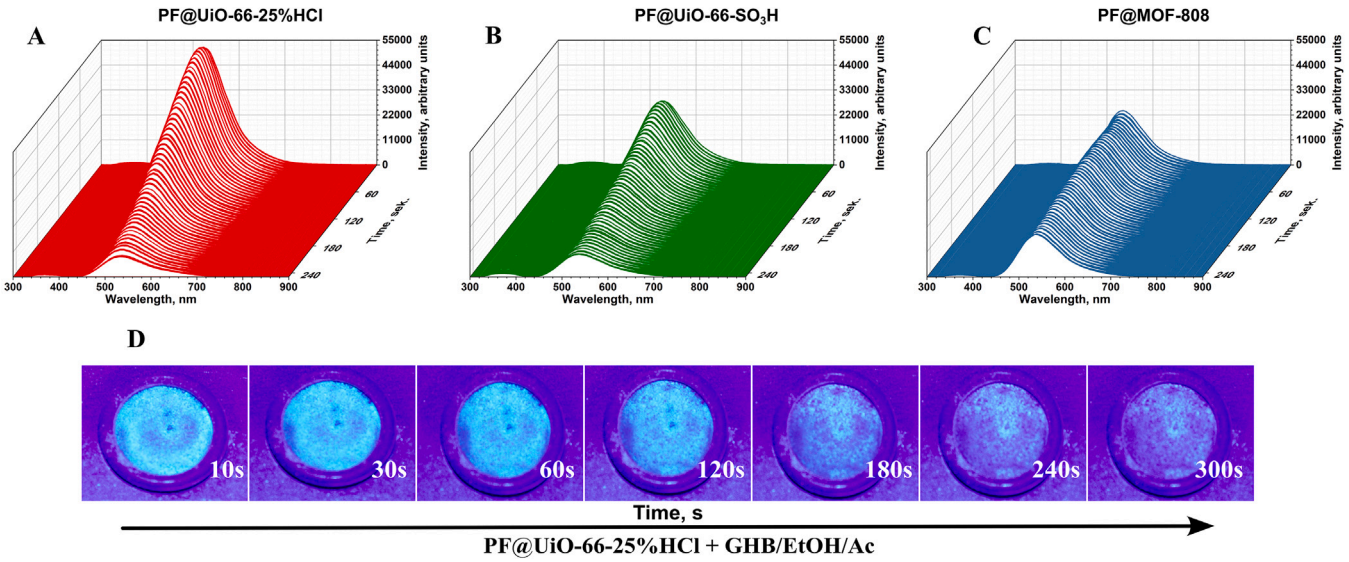

Fig. 7. Kinetics of luminescence for PF@MOF composites and the mixture of GHB/EtOH/Ace addition upon excitation at 365 nm (**A-C**); (**A**) PF@UiO-66-25%HCl; (**B**) PF@UiO-66-SO_3H (**C**) PF@MOF-808. (**D**) Time variation of luminescence for PF@UiO-66-25%HCl probe after GHB/EtOH/Ace addition upon excitation at 455 nm. Photos were taken after 10 s, 30 s, 60 s, 120 s, 180 s, 240 s, and 300 s.

of PF@MOF probes in GHB detection and to demonstrate the lack of performance for both dye and pristine MOFs. According to the images in Figures S14-B, D, and F (Supporting Information file), it is apparent that there is no change in luminescence, regardless of the type of MOF. The addition of the solvent in the form of EtOH, Ace, drug GHB-Na, and a mixture of drug and solvent, or a mixture of solvents, does not cause any visible change. Under the LED light, MOFs appear white to the "naked eye" and in the camera objective. These results agree with the spectrofluorometric measurements presented in Fig. 6 and Figure S12 and discussed in the "spectrofluorometric measurement" subsection. The results indicate that the pristine MOF does not exhibit GHB-Na detection capability and cannot be used for this purpose. An expressive lack of change under the influence of the drug is observable. A similar relationship was observed for PF dye (Figure S14-G). The addition of the mentioned solvents and GHB-Na did not affect the PF dye. We do not observe any changes in PF luminescence; only wet spots from the added solvents and mixtures are visible. With the addition of Ace, we observe a slight luminescence of the material, but it is barely visible. This may be related to the dissolution of the dye under the influence of added acetone. The same relationship was observed for pristine MOFs (Figure S14-B,D,F). The materials do not show luminescence but appear white and glowing under the light of 455 nm wavelength. It is due to the reflection of light by these materials. However, it is not luminescence caused by the addition of solvents and/or GHB-Na. The luminescence effect itself is different from that seen for PF@MOFs, making it easy to distinguish. Interestingly, in the spectrofluorometric spectra, we observe a change in wavelength for the band of maximum intensity upon the addition of GHB-Na/EtOH/Ace. This means that by using instrumental methods, we can document and confirm the addition of GHB-Na. However, without specialized apparatus, the presence of GHB-Na cannot be confirmed. The PF@UiO-66-25%HCl probe was selected as the most effective and sensitive of all those tested. In this case, the leading one is very slight and suppressed luminescence under Ace, and more intense when EtOH alone or GHB-Na alone is added. Nevertheless, this is the addition of GHB-Na/EtOH and GHB-Na/EtOH/Ace that significantly changes the color and intensity of the sample's luminescence. Especially in the last case, it is extremely intense and takes on a fluorescent green color. The visual effect is of a wider variety than for the other cases, both without and after the addition of GHB-Na. This makes it possible to confirm the presence of the added drug reliably or ensure its absolute absence. Luminescence is possible with the "naked eye", and the significant difference excludes the possibility of a mistake in GHB addition (Figure S14-A). Moreover, the luminescence effect persists for up to 5 min. Fig. 7D shows the attenuation of luminescence of PF@UiO-66-25%HCl with GHB/EtOH/Ace addition at 5 min. We observe a very pronounced luminescence of the sample and no weakening of the luminescence effect for 2 min after the addition of the mixture. Then, the luminescence is slightly dimmed and loses intensity, but remains visible and noticeable. After 5 min, the luminescence gradually extinguished. Such a long luminescence time, and thus a persistent effect, further facilitates the detection of the presence or absence of GHB-Na, given real, everyday situations, e.g., in nightclubs. These results are consistent with spectrofluorometric measurements, where a slight wavelength shift from 510 nm to 515 nm was observed. The PF@UiO-66-SO_3H probe showed less selective performance. In this case, we observe luminescence already upon the addition of solvents, like acetone or ethanol, and GHB-Na. The addition of the GHB-Na/EtOH/Ace mixture also leads to a change in both color and intensity, although the effect is not as pronounced as for PF@UiO-66-25%HCl. Nevertheless, it is possible to confirm the presence of GHB-Na with this composite as well (Figure S14-C). A similar relationship is observable on the emission spectrum, where the wavelength change is also smaller than for PF@UiO-66-25%HCl. For PF@MOF-808 (Figure S14-E), the addition of ethanol or acetone causes weak luminescence, but only upon the addition of GHB-Na/EtOH/Ace was the intense luminescence visible. In addition, a slight color change to an intense green, as in the previously discussed cases, was also observed. However, the changes are faintly visible here, and the intensity is not as significant as in PF@UiO-66-25%HCl. This means that drug detection is possible and the probe's operation is reasonable, albeit it is not as specific as the previous ones, as shown in Figure S14-A, C, E. Additionally, there is no change in the emission spectrum, which emphasizes its weak performance. The results obtained are significant and forward-looking. The designed PF@MOFs probes can be potential detectors of GHB-Na in solutions, including alcoholic solutions, where it is most often added. The PF@UIO-66-25%HCl probe reveals the highest efficiency and selectivity due to its marked luminescence, color change upon addition of GHB-Na/EtOH/Ace, and very long luminescence effect lasting as long as more than 5 min. For PF@UiO-66-SO_3H and PF@MOF-808, the effect is less distinct, but luminescence under the influence of the mixture mentioned above occurs, and changes were observable.

However, they can be difficult to observe with the naked eye in a short time.

To assess the practical applicability of the designed PF@MOF probes for real-world detection, an experiment was conducted to evaluate their luminescence response upon exposure to GHB-Na and relevant solvents. The study was performed in a darkened chamber using a light-emitting diode (LED) with an excitation wavelength of 455 nm. Both fluorescent MOF probes (PF@UiO-66-25%HCl, PF@UiO-66-SO_3H, and PF@MOF-808) and their respective pristine MOF counterparts (UiO-66-25%HCl, UiO-66-SO_3H, and MOF-808), as well as PF dye, were examined. This experimental design aimed to establish the specificity of PF@MOF composites in GHB detection while simultaneously demonstrating that neither the pristine MOFs nor the dye alone could facilitate such detection. The results, illustrated in Figures S14-B, D, and F, reveal that pristine MOFs exhibit no visible luminescence changes, regardless of the solvent used. Adding EtOH, Ace, GHB-Na, or their mixtures does not induce any observable alterations. Under LED illumination, all MOFs appear white to the naked eye and in the camera images. These findings align with the spectrofluorometric measurements (Figure S14) and corroborate the conclusion that pristine MOFs do not possess the capability to detect GHB-Na. The lack of luminescence response under the influence of GHB-Na further confirms their ineffectiveness in this application.

A similar trend was observed for PF dye (Figure S14-G). The introduction of solvents or GHB-Na did not lead to any discernible luminescence changes; only the formation of wet spots from the added substances was apparent. The addition of acetone resulted in a slight increase in luminescence intensity, though it remained faint and difficult to detect. This phenomenon is likely attributable to the partial dissolution of the dye in acetone. Notably, while spectrofluorometric spectra demonstrated a shift in the wavelength of maximum intensity upon the addition of GHB-Na/EtOH/Ace, no such change was perceptible to the naked eye. This underscores the necessity of instrumental analysis for unequivocal confirmation of GHB-Na presence.

Among the tested probes, PF@UiO-66-25%HCl exhibited the highest sensitivity and selectivity. The probe displayed weak but noticeable luminescence in the presence of acetone, which intensified upon exposure to EtOH or GHB-Na alone. However, the most significant luminescence enhancement and color change occurred when GHB-Na/EtOH or GHB-Na/EtOH/Ace was added. In the latter case, the sample exhibited a striking fluorescent green hue, markedly different from all other conditions, in either absence or presence of GHB-Na. This pronounced visual effect enables reliable, unaided detection of the drug's presence or its definitive exclusion. Importantly, the luminescence was readily observable with the naked eye, and the contrast was sufficiently distinct to minimize the risk of misinterpretation (Figure S14-A). More importantly, the luminescence effect persisted for up to five minutes. Fig. 7D illustrates the decay of PF@UiO-66-25%HCl luminescence following the addition of GHB/EtOH/Ace. The luminescence remained intense for at least two minutes post-exposure, showing no immediate weakening. Gradual dimming was observed thereafter, yet the luminescence remained clearly visible even at the five-minute mark. This extended luminescence duration enhances the practicality of the probe for real-world applications, such as nightclubs, where rapid and reliable detection is crucial from a safety point of view. The PF@UiO-66-SO_3H probe demonstrated lower selectivity compared to PF@UiO-66-25%HCl. Luminescence was already apparent upon the addition of solvents (acetone or ethanol), as well as GHB-Na. However, exposure to the GHB-Na/EtOH/Ace mixture still resulted in a noticeable change in both luminescence intensity and color, albeit less pronounced than for PF@UiO-66-25%HCl. Despite this reduced selectivity, the probe remained capable of GHB-Na detection (Figure S14-C). A corresponding shift was observed in the emission spectrum, although smaller than that recorded for PF@UiO-66-25%HCl.

In the case of PF@MOF-808, weak luminescence was detected upon addition of ethanol or acetone. However, significant luminescence enhancement and a slight green color shift were only observed upon exposure to GHB-Na/EtOH/Ace. While this probe enables GHB-Na detection, the luminescence effect is less intense and less distinct compared to PF@UiO-66-25%HCl and PF@UiO-66-SO_3H. Additionally, no substantial shift in the emission spectrum was recorded, further emphasizing its lower performance in selective drug detection.

PF@MOF composite contains PF adsorbed in MOF. The surface charge of this complex (PF@UiO-66-25%HCl and PF@MOF-808) is positive. The dye itself contains two amine groups and a heterocyclic nitrogen atom. GHB shows a negative charge due to the presence of carboxyl groups. In aqueous solution, carboxyl and amine groups are ionized. Two opposite charges emerged, attracting each other and forming a hydrogen bond. This may affect the ability to detect GHB with PF@MOF fluorescent probes. The addition of ethanol and acetone increases the luminescence intensity of the sample due to the dissolution of the dye, thus increasing the visual effect of detection. In addition, both ethanol and acetone, although polar solvents, are less polar than water. This causes them to be less competitive in forming hydrogen bonds, unlike water. This favors the formation of a bond between –COOH in GHB and –NH_2 in PF. This enhances the probe's detection capabilities. Although this is not a requirement for GHB-induced probe luminescence, it is helpful for identification, due to the intensity of the luminescence and the persistent effect, up to 5 min (Fig. 7). Luminescence of the probe is also observable for GHB dissolved in water, but it lasts no longer than 1 min. Ethanol and acetone alone can cause the sample to exhibit luminescence, and the color and intensity of the probe are different, as shown in Figure S14, and are related to the dissolution of the PF dye. Moreover, the luminescence effect disappears quickly and does not persist. There is an observable change in the color, intensity, and luminescence elongation of the PF@MOF probe under the influence of GHB and organic solvents. PF@UiO-66-SO_3H does not show selectivity, which may be due to the negative surface charge of the metal–organic framework. This underscores the validity of the presented mechanism.[20]

Much higher detection capabilities were observed when the MOF did not have a functionalized surface, i.e., for UiO-66-25%HCL and MOF-808. These MOFs have a positive surface charge due to the presence of metallic clusters. After attachment of the neutral PF dye, the charge remains positive. The resulting PF@UiO-66-25%HCl and PF@MOF-808 complexes have an adsorbed dye with an amine group and a heterocyclic atom. Under the influence of solvents, the composite shows a positive charge. Dissolved GHB has a negative charge. There is an interaction between the dye and the composite, and the formation of a hydrogen bond. On the other hand, functionalizing the MOF surface with sulfone groups UiO-66-SO_3H changes the surface charge to negative. The attachment of the dye still does not change the charge but only makes it more inert. The composite-GHB interaction is then weakened, reducing the detection capability of the PF@UiO-66-SO_3H fluorescent probe. The characteristic luminescence of the sample upon the addition of GHB and organic solvents does not occur, as shown in Figure S14.

In conclusion, MOFs with no functional groups on the surface and those with a positive surface charge are much more selective for rape tablet detection.

3.6. GHB-Na sorption process

Besides the applicability of MOF structures as hosts for chemical sensors to detect the presence of GHB-Na in a liquid environment, they exhibit a high affinity for the adsorption of GHB-Na molecules. To determine the sorption ability of the considered materials, Monte Carlo classical force-field modeling was performed. The most stable structures were reoptimized at the DFT level. The adsorption energies, together with the charges (two population analyses: Bader and DDEC6) and bond orders (DDEC6), are summarized in Table 2.

The strongest adsorption was found for the GHB@UiO-66_str1 localization, with the total bond order between the GHB molecule and the

Table 2
Adsorption energies of GHB in the MOF UiO-66 and MOF-808 frameworks. The total bond order, *BO*(GHB-MOF), between the adsorbed molecule and the host MOF framework is determined using the DDEC6 bond analysis. The accumulated charge on the adsorbate molecule, q_{DDEC}(GHB) and q_{Bader}(GHB), were calculated via the DDEC6 and the Bader partial charge analyses, respectively.

Adsorbate molecule	E_{ads}/eV	*BO*(GHB-MOF)	q_{DDEC}(GHB)	q_{Bader}(GHB)
GHB@UiO-66_str1	−0.846	0.7059	0.0488	0.0426
GHB@UiO-66_str2	−0.577	0.5354	0.0351	−0.0015
GHB@UiO-66_str3	−0.788	0.7711	0.0717	0.0538
GHB@MOF-808_str1	−0.573	0.6305	−0.0355	−0.0079
GHB@MOF-808_str2	−0.777	0.7306	0.0744	0.0167
GHB@MOF-808_str3	−0.903	0.8953	0.0704	0.0228
GHB@MOF-808_str4	−0.389	0.3797	0.0224	−0.0029

MOF framework equal to ca. 0.7. The interaction is mostly covalent, and the overall charge transfer between the adsorbate molecule and the host structure is low, ca. 0.04. For the other geometry (GHB@UiO-66_str3), the adsorption is only slightly weaker (by ca. 0.06 eV), and the bond order is a little higher. The accumulated charge is also very low. The third geometry (GHB@UiO-66_str2) corresponds to the weakest interactions and also to the lowest bond order.

For the sorption in MOF-808, the energetic discrimination is much more pronounced: for GHB@MOF-808_str3 the adsorption energy is equal to −0.903 eV, while for GHB@MOF-808_str4 it is only −0.389 eV. The bond orders are 0.8953 and 0.3797, respectively. The charge transfer is also very weak and does not exceed 0.075 |e|.

The most stable DFT-optimized structures of GHB@UiO-66 and GHB@MOF-808 are presented in Fig. 8, while the other geometries of local energy minima are presented in the Supporting Information file (Figures S15-S19).

The equilibrium loading was estimated by the Monte-Carlo simulations at a temperature of 298 K, with use of the Metropolis algorithm and the Universal Force Field [84]. The isotherms were modeled for the fugacity up to 100 kPa. The rigid host approximation was used, which can rationalize the underestimation of the modeled loading for the MOF structures with tight channels. Out of the structures predicted by the MC simulations, those nonequivalent by symmetry were further re-optimized at the DFT/DFTsol levels of theory (Table 3).

The adsorption energy in the polarizable continuum (mimicking the presence of the solvent with a dielectric constant of 80) relative to their adsorption energies in vacuum for the sequence of GHB@UiO-66 adsorbates is 0.349, 0.150, and 0.244.

For MOF-808, the diversification of the adsorption energies among the studied geometries is twice as high (compared to sorption of GHB in UiO-66), up to ca. 0.5 eV (0.246, 0.226, 0.389, and 0.117 for the sequence of geometries). Again, the introduction of a polar environment does not significantly change the order of energies.

Interestingly, the most stable structure in a vacuum is the strongest destabilized by the solvent, but the resultant trend in the adsorption energies in the solvent remains almost unchanged. This does not predestine, however, the solubility in less polar solvent for the interaction of the alkyl part of the GHB molecule with the non-polar part of the solvent molecules also contributes to the solubility of GHB and, taking into account also the competitive affinity of the solvent molecules to the MOF framework, the elution of GHB by less polar solvents can be more effective compared to water [85].

To determine GHB-Na sorption efficiency on prepared MOF samples, the sorption experiments were performed in water and a 20% alcoholic environment (Fig. 9). When deionized water was used as a liquid environment medium, the UiO-66-25%HCl revealed the highest GHB-Na sorption capacity, reaching 2430 mg of GHB per 1 g of MOF adsorption after 24 h. In the case of UiO-66-SO_3H and MOF-808, the maximum sorption was also reached after 24 h and was equal to 1937 mg and 1398 mg per 1 g of MOF, respectively. The effect of EtOH on the adsorption process was observed; however, it depended on the type of MOF used. Adsorption of GHB-Na in an alcoholic solution using UiO-66-25%HCl is inhibited, resulting in a reduction in the amount of drug removed from the solution. In the 20% EtOH solution, the maximum adsorbed value of GHB-Na was 1910 mg per 1 g of MOF. For the other MOF materials, the opposite relationship was observed. In the case of UiO-66-SO_3H and MOF-808, higher adsorption values of GHB-Na were achieved, reaching 3112 mg and 3003 mg of GHB-Na absorbed by 1 g of the MOF used, respectively.

The influence of increased temperature and EtOH content on the adsorption efficiency of MOFs was previously reported in the literature [86,88,89]. It is noteworthy that for low concentrations of ethanol, the dielectric constant of the solvent is only slightly lower than for water, e.g., for 20% EtOH solution in water, ε = 71.23 [85]. It has been confirmed that temperature has a more significant effect on the adsorption process than the addition of ethanol alone. Nevertheless, increasing the percentage of ethanol in the medium reduces the material's sorption capacity. This is due to the possibility of the organic molecule entering the pores of the MOF and, due to its small size, competing with comparably small and polar GHB molecules, causing a reduction in the amount of drug adsorption [88]. Electrostatic interaction between the charges of the atoms in the medium can occur [86]. Such a situation is observed for UiO-66-25%HCl. The sorption capacity is improved for UiO-66-SO_3H and MOF-808. We can surmise that there is an interaction of ethanol with a sulfonic group, located on the surface of MOF in the case of UiO-66-SO_3H, and an extensive ligand, containing three carboxyl groups, in the case of MOF-808. Then, ethanol interacts with the elements mentioned above, which do not limit or inhibit the adsorption process of GHB. In this case, we see that the molecule is absorbed more efficiently. Thus, we can explain this effect by the interaction of the medium with the MOF skeleton; water does not interact with its pores but only with the network, so that the GHB molecule can be more easily adsorbed and removed from the environment [86,88,89]. For sorption processes in both water and ethanol, the kinetics profiles were determined. Each of the discussed cases fits pseudo-second-order kinetics, as shown in Figure S20.

The specific surface area of UiO-66-SO_3H is the lowest among the MOFs discussed and is equal to 198 m^2 g^{-1}. However, this MOF shows high sorption capacity for GHB-Na adsorption, much higher than MOF-808, whose S_{BET} is 1130 m^2 g^{-1} (adsorption in H_2O), and higher than for UiO-66-25%HCl for adsorption in 20% EtOH, whose specific surface area reaches 1057 m^2 g^{-1}. The exceptional sorption capacity of UiO-66-SO_3H is related to the presence of the –SO_3H group on the surface of the metal–organic framework. The sulfonic group can indeed get ionized (forming –SO_3^-) in aqueous solutions and act as additional adsorption sites. Changing the surface charge of the metal–organic framework to negative can result in more efficient adsorption of molecules. Although the specific surface area of the structure decreases, it is enriched with additional groups generating adsorption sites. Adsorption is also easier due to the presence of groups on the surface. The –SO_3H group has a high affinity for positively charged molecules, such as the GHB-Na discussed in the experiment.[90,91]

3.7. Detection mechanism

The article of Y. Zhang et al. [47] discusses possible modes of fluorescence in MOF structures loaded with guest molecules and summarizes that the luminescence in such systems primarily originates from metal nodes, organic linkers, and guest molecules adsorbed in the pores. Additionally, LMCT – ligand–to–metal charge transfer; MLCT - metal–to–ligand charge, and LLCT–ligand–to–ligand transfer processes may occur. The possible mechanisms of the fluorescence processes observed in MOFs are summarized in Fig. 10A.

It must also be emphasized that in the case of PF@MOF samples, the fluorescence mechanism must also consider additional fluorescence from the PF molecule, which includes additional MLCT, LMCT, and LLCT processes.

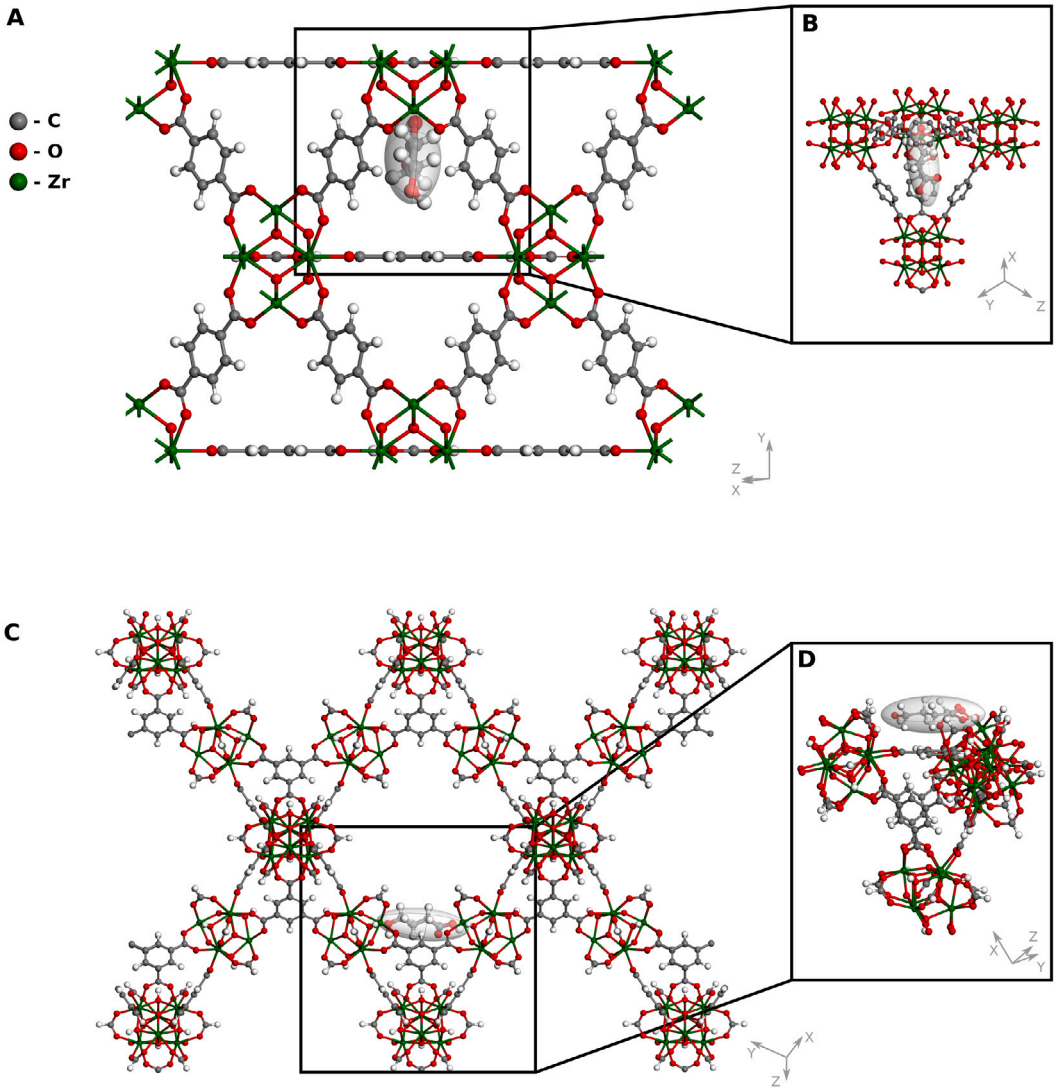

Fig. 8. DFT optimized structure of GHB@UiO-66_str1 (panels **A**, **B**) and GHB@MOF-808_str3 (panels **C**, **D**) with GHB molecule marked with ellipsoid; (**A**, **C**): general model, (**B**, **D**): zoomed channel with adsorbed GHB; coloring: green — Zr, red — O, gray — C, white — H. Additional structures are provided in the Supplementary Information File.

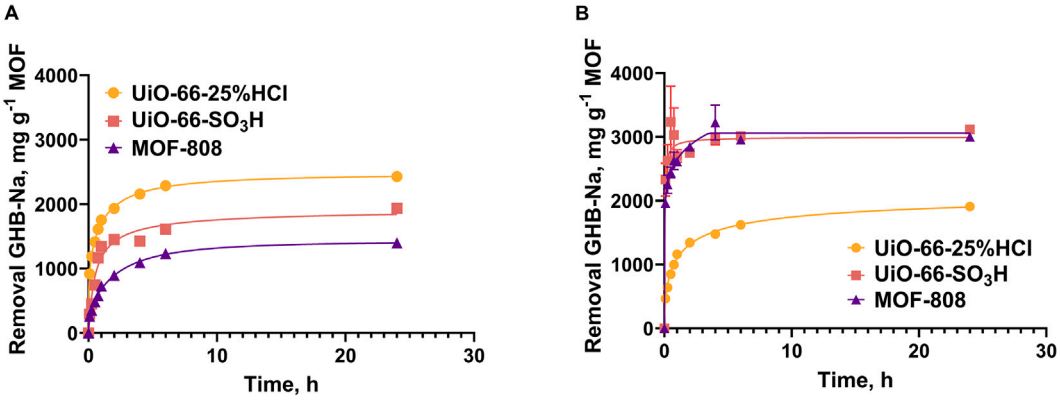

Fig. 9. GHB-Na removal in different media (**A**) distilled water; (**B**) 20% EtOH solution.

Table 3
Energetics of GHB sorption in studied MOF structures in dry (DFT) and aqueous (DFTsol, polarizable continuum with $\epsilon = 80$) environments. The calculated loading $n_{molecules}$ was estimated per 1 unit cell of MOF.

Adsorbates	E_{ads} (vac.) / eV	E_{ads} (water) / eV	$n_{molecules}$ (*) (calc.)	$n_{molecules}$ (*) (exp.)
GHB@UiO-66_1	−0.846	−0.497	12.0 (3.0); 2.12 wt%	51.7/ 41.2 wt.%(***)
GHB@UiO-66_2	−0.577	−0.427		
GHB@UiO-66_3	−0.788	−0.544		
GHB@MOF-808_1	−0.573	−0.327	32 (8.0); 37.9 wt%	29.8 wt%
GHB@MOF-808_2	−0.777	−0.551		
GHB@MOF-808_3	−0.903	−0.514		
GHB@MOF-808_4	−0.389	−0.272		

* calculated by MC within the rigid host approximation (in parentheses: per a single Zr_6 cluster); after semicolon, the weight percentage of GHB in MOF framework is given.
** values calculated from the experimental wt.%.
*** Experimental results were obtained for UiO-66-25%HCl, hence, they should not be compared to the results of modeling.

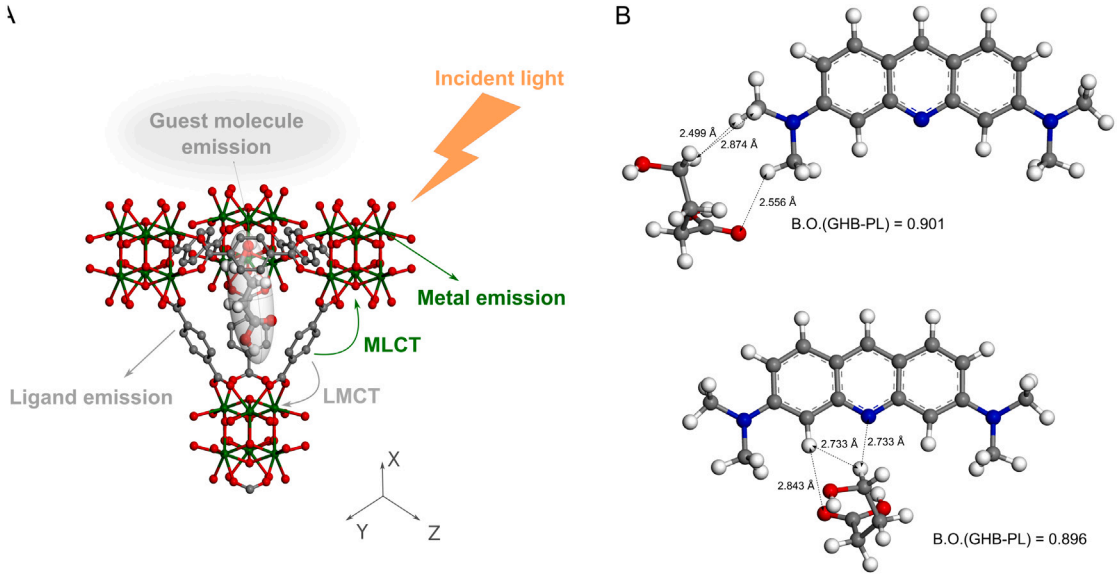

Fig. 10. (**A**) Representation of possible emission modes in MOFs. GHB molecule marked with ellipsoid; LMCT — ligand-to-metal charge transfer; MLCT — metal-to-ligand charge transfer; coloring: green — Zr, red — O, gray — C. Hydrogens omitted for clarity. (**B**) Ground state DFTsol/B3LYP optimized geometries of the GHB-PL structure 1 (top) and 2 (bottom). The total bond order between the two molecules is denoted B.O.(GHB-PL). Distances shorter than 3.0 Åare shown as arrows.

As shown in the emission spectra (Fig. S21), the perturbation of the PF electronic structure by GHB, assisted by the MOF framework, increases the intensity of emission several-fold. While the charge transfer between the GHB molecule and the MOF frameworks (Table 2) is very low (0.02–0.07 |e|), the bond order is relatively high, in the range of 0.4–0.9 at. u. The closest contacts between the GHB and PL molecules are shown in Fig. 10B. Thus, the increase in fluorescence process can be attributed to the interaction of the electronic structures of all counterparts. The overlap, and hence interaction, between the electronic structures of PF, MOF, and GHB-Na increases the transition moment for fluorescence, and, consequently, its intensity, and shifts the wavelength.

Another factor intensifying the fluorescence is the increase in the concentration of GHB-Na adsorbed in MOFs in alcoholic environments (shown here both computationally and experimentally).

As already discussed in Y. Zhang et al. [47], four different types of fluorescence, including turn-on-emission enhancement, turn-off-emission decrease, emission shift, and a combination of the first two mechanisms with the third one, are postulated. Since the first two mechanisms are evident and already confirmed by the experiments in this study, the third type was partially confirmed via μRaman spectroscopy (cf. Fig. 5D) for PF@UiO-66-25%HCl and PF@UiO-66-SO_3H samples.

Since the fluorescence mechanisms observed in this study are complex, the direct determination of the detection mechanism in PF@MOF samples would require a much detailed study which goes far beyond the scope of this manuscript.

4. Conclusions

This paper presents a series of fluorescent probes based on zirconium-based metal–organic frameworks (MOFs) and proflavine (PF) dye for the detection of GHB-Na, commonly referred to as the “date-rape pill”.

The differences in detection efficiency were assessed by varying the molecular and structural properties of the synthesized samples. To obtain the fluorescent probes, the fluorescent PF dye was incorporated into various Zr-MOF frameworks from the UiO-66 family, including UiO-66-25%HCl, functionalized UiO-66-SO_3H, and MOF-808. The efficiency of GHB-Na detection was evaluated through spectrofluorimetric measurements and “naked eye” detection. Spectrofluorometric analysis allowed for the observation of emission and excitation spectra, highlighting significant differences upon the addition of solvents, GHB-Na, and a mixture of GHB-Na with solvents. A particularly notable difference was observed when a mixture of GHB/EtOH/Ace was added

to the probe, where the addition of acetone increased the intensity of the emission band. Furthermore, the simultaneous addition of acetone and ethanol resulted in a considerable wavelength shift of the maximum intensity band in the presence of GHB-Na. This shift was absent when GHB-Na was not present. The PF@UiO-66-25%HCl composite exhibited the largest shift and change in the band intensity, while no shift was observed for PF@MOF-808. Luminescence kinetics revealed a relatively long luminescence life for the examined samples, with the highest luminescence intensities observed for PF@UiO-66-25%HCl, almost double that of PF@UiO-66-SO_3H. While luminescence persisted for up to 4 min, it gradually diminished and exhibited weaker intensities. For PF@MOF-808, no significant reduction in luminescence was noticed after 4 min. In the "naked eye" detection, upon adding the GHB/EtOH/Ace mixture, a bright fluorescent-green luminescence was observed for PF@UiO-66-25%HCl composite. Under the influence of solvent addition alone, luminescence was not detected, while GHB alone resulted in a less distinct luminescence. In addition to the remarkable fluorescent properties of the prepared PF@MOF composites, their enhanced GHB-Na sorption capabilities were also confirmed. An increase in GHB-Na sorption efficiency in an ethanolic solution was observed for UiO-66-SO_3H and MOF-808, while a slight decrease was noted for UiO-66-25%HCl sample. This may be attributed to the interaction of ethanol and water with the lattice backbone, which may inhibit molecules from penetrating the MOFs, thereby affecting the accessibility of GHB-Na to the pores. The UiO-66-25%HCl exhibited the highest sorption efficiency in distilled water, whereas UiO-66-SO_3H demonstrated superior efficiency in ethanol. The feasibility and effectiveness were also confirmed on the actual beverages. The research presented a route to quickly confirm the addition of GHB-Na, both from the chemical side, through the analysis of emission and excitation spectra, as well as a simple evaluation of the sample's luminescence, making the method accessible to everyone and requiring no specialized knowledge.

CRediT authorship contribution statement

Kornelia Hyjek: Methodology, Validation, Formal analysis, Investigation, Resources, Data Curation, Writing – original draft, Writing – review & editing, Visualization. **Grzegorz Kurowski:** Investigation. **Anna Pajdak:** Investigation, Resources, Data Curation, Writing – original draft, Writing – review & editing, Visualization. **Łukasz Kuterasiński:** Investigation. **Sylwia Tomczyk:** Investigation. **Klaudia Jasińska:** Investigation. **Patryk Szymaszek:** Investigation. **Joanna Ortyl:** Investigation. **Piotr Jeleń:** Investigation. **Maciej Sitarz:** Investigation. **Witold Piskorz:** Methodology, Validation, Formal analysis, Investigation, Resources, Data Curation, Writing – original draft, Writing – review & editing, Visualization, Software. **Przemysław J. Jodłowski:** Conceptualization, Methodology, Validation, Formal analysis, Investigation, Resources, Data Curation, Writing – original draft, Writing – review & editing, Visualization, Supervision, Funding acquisition.

Declaration of competing interest

The authors declare that they have no known competing financial interests or personal relationships that could have appeared to influence the work reported in this paper.

Acknowledgments

The work was supported by the National Science Centre, Poland, under the research project "MOF-antidote: Novel detoxification materials based on metal–organic frameworks for drugs of abuse removal – synthesis, chemical characterization, toxicity, and efficacy in vivo and in vitro studies", no. UMO-2021/43/B/NZ7/00827.

We gratefully acknowledge the Polish high-performance computing infrastructure PLGrid (HPC Center: ACK Cyfronet AGH) for providing computer facilities and support within computational grant no. PLG/2025/018368.

Appendix A. Supplementary data

Supplementary material related to this article can be found online at https://doi.org/10.1016/j.saa.2025.127375.

Data availability

Hyjek, Kornelia; Kurowski, Grzegorz; Pajdak, Anna; Kuterasiński, Łukasz; Tomczyk, Sylwia; Jasińska, Klaudia; Szymaszek, Patryk; Ortyl, Joanna; Jeleń, Piotr; Sitarz, Maciej; Piskorz, Witold; Jodłowski, Przemysław (2025), "MOF-Integrated Fluorescent Composites and Adsorbents for Rapid Detection and Removal of Date-Rape Drugs", Mendeley Data, V1, doi: 10.17632/cwrv4c7n9f.1.

References

[1] J. Mead, A. Parrott, Mephedrone and MDMA: A comparative review, Brain Res. 1735 (2020) 146740, http://dx.doi.org/10.1016/j.brainres.2020.146740, URL https://linkinghub.elsevier.com/retrieve/pii/S0006899320300962.

[2] S. Berman, J. O'Neill, S. Fears, G. Bartzokis, E.D. London, Abuse of amphetamines and structural abnormalities in the brain, Ann. New York Acad. Sci. 1141 (1) (2008) 195–220, http://dx.doi.org/10.1196/annals.1441.031, URL https://nyaspubs.onlinelibrary.wiley.com/doi/10.1196/annals.1441.031.

[3] I.M. Ornelas, F.A. Cini, I. Wießner, E. Marcos, D.B. Araújo, L. Goto-Silva, J. Nascimento, S.R.B. Silva, M.N. Costa, M. Falchi, R. Olivieri, F. Palhano-Fontes, E. Sequerra, D. Martins-de Souza, A. Feilding, C. Rennó-Costa, L.F. Tófoli, S.K. Rehen, S. Ribeiro, Nootropic effects of LSD: Behavioral, molecular and computational evidence, Exp. Neurol. 356 (2022) 114148, http://dx.doi.org/10.1016/j.expneurol.2022.114148, URL https://linkinghub.elsevier.com/retrieve/pii/S001448862200173X.

[4] I. Straumann, L. Ley, F. Holze, A.M. Becker, A. Klaiber, U. Duthaler, N. Varghese, A. Eckert, M.E. Liechti, Acute effects of MDMA and LSD co-administration in healthy participants, Neurosci. Appl. 2 (2023) 103381, http://dx.doi.org/10.1016/j.nsa.2023.103381, URL https://linkinghub.elsevier.com/retrieve/pii/S2772408523023633.

[5] J. Listos, M. Łupina, S. Talarek, A. Mazur, J. Orzelska-Górka, J. Kotlińska, The mechanisms involved in morphine addiction: An overview, Int. J. Mol. Sci. 20 (17) (2019) 4302, http://dx.doi.org/10.3390/ijms20174302, URL https://www.mdpi.com/1422-0067/20/17/4302.

[6] G. Petruševski, J. Acevska, G. Stefkov, A.P. Panovska, I. Micovski, R. Petkovska, A. Dimitrovska, S. Ugarkovic, Characterization and origin differentiation of morphine derivatives by DSC/TG and FTIR analysis using pattern recognition techniques, J. Therm. Anal. Calorim. 123 (3) (2016) 2561–2571, http://dx.doi.org/10.1007/s10973-016-5242-z, URL http://link.springer.com/10.1007/s10973-016-5242-z.

[7] J.R. Weeks, Experimental morphine addiction: Method for automatic intravenous injections in unrestrained rats, Science 138 (3537) (1962) 143–144, http://dx.doi.org/10.1126/science.138.3537.143, URL https://www.science.org/doi/10.1126/science.138.3537.143.

[8] T.S.T. Balamurugan, K. Kwaczyński, M. Rizwan, L. Poltorak, Current trends in rapid electroanalytical screening of date rape drugs in beverages, TrAC Trends Anal. Chem. 175 (2024) 117712, http://dx.doi.org/10.1016/j.trac.2024.117712, URL https://linkinghub.elsevier.com/retrieve/pii/S0165993624001948.

[9] S. Abanades, F. Magí, M. Segura, S. Pichini, D. Barral, R. Pacifici, M. Pellegrini, F. Fonseca, K. Langohr, R. De La Torre, γ-Hydroxybutyrate (GHB) in humans, Ann. New York Acad. Sci. 1074 (1) (2006) 559–576, http://dx.doi.org/10.1196/annals.1369.065, URL https://nyaspubs.onlinelibrary.wiley.com/doi/10.1196/annals.1369.065.

[10] V.L. Brewster, H.G.M. Edwards, M.D. Hargreaves, T. Munshi, Identification of the date-rape drug GHB and its precursor GBL by Raman spectroscopy, Drug Test. Anal. 1 (1) (2009) 25–31, http://dx.doi.org/10.1002/dta.11, URL https://analyticalsciencejournals.onlinelibrary.wiley.com/doi/10.1002/dta.11.

[11] M. Grootveld, D. Algeo, C.J.L. Silwood, J.C. Blackburn, A.D. Clark, Determination of the illicit drug gamma-hydroxybutyrate (GHB) in human saliva and beverages by 1H NMR analysis, BioFactors 27 (1–4) (2006) 121–136, http://dx.doi.org/10.1002/biof.5520270111, URL https://iubmb.onlinelibrary.wiley.com/doi/10.1002/biof.5520270111.

[12] G.P. Galloway, S.L. Frederick, F.E. Staggers, M. Gonzales, S.A. Stalcup, D.E. Smith, Gamma-hydroxybutyrate: an emerging drug of abuse that causes physical dependence, Addiction 92 (1) (1997) 89–96, http://dx.doi.org/10.1111/j.1360-0443.1997.tb03640.x, URL https://onlinelibrary.wiley.com/doi/10.1111/j.1360-0443.1997.tb03640.x.

[13] S. Rodríguez-Nuévalos, A.M. Costero, M. Parra, S. Gil, P. Arroyo, J.A. Sáez, P. Gaviña, P. Ceroni, A. Fermi, Colorimetric and fluorescent hydrazone-BODIPY probes for the detection of γ-hydroxybutyric acid (GHB) and cathinones, Dye. Pigment. 207 (2022) 110757, http://dx.doi.org/10.1016/j.dyepig.2022.110757, URL https://linkinghub.elsevier.com/retrieve/pii/S0143720822006799.

[14] E. Garrido, G. Hernández-Sigüenza, E. Climent, M.D. Marcos, K. Rurack, P. Gaviña, M. Parra, F. Sancenón, V. Martí-Centelles, R. Martínez-Máñez, Strip-based lateral flow-type indicator displacement assay for γ-hydroxybutyric acid (GHB) detection in beverages, Sensors Actuators B Chem. 377 (2023) 133043, http://dx.doi.org/10.1016/j.snb.2022.133043, URL https://linkinghub.elsevier.com/retrieve/pii/S0925400522016860.

[15] S.U. Son, S. Jang, B. Kang, J. Kim, J. Lim, S. Seo, T. Kang, J. Jung, K.-S. Lee, H. Kim, E.-K. Lim, Colorimetric paper sensor for visual detection of date-rape drug γ-hydroxybutyric acid (GHB), Sensors Actuators B Chem. 347 (2021) 130598, http://dx.doi.org/10.1016/j.snb.2021.130598, URL https://linkinghub.elsevier.com/retrieve/pii/S0925400521011667.

[16] M. Hu, Q. Han, B. Xing, Metallic nanoparticle-enabled sensing of a drug-of-abuse: An attempt at forensic application, ChemBioChem 21 (17) (2020) 2512–2517, http://dx.doi.org/10.1002/cbic.202000157, URL https://chemistry-europe.onlinelibrary.wiley.com/doi/10.1002/cbic.202000157.

[17] R. Paul, L. Tsanaclis, R. Kingston, A. Berry, A. Guwy, Simultaneous determination of GHB and EtG in hair using GCMS/MS, Drug Test. Anal. 3 (4) (2011) 201–205, http://dx.doi.org/10.1002/dta.172.

[18] R.R. Hughes, G.S. Walker, Rapid screening for the detection and differentiation of Gamma-hydroxybutyrate using ion chromatography, J. Forensic Sci. 56 (5) (2011) 1256–1260, http://dx.doi.org/10.1111/j.1556-4029.2011.01845.x, URL https://onlinelibrary.wiley.com/doi/10.1111/j.1556-4029.2011.01845.x.

[19] G.-J. Kim, S.J. Park, L. Kim, K.H. Kim, S. Kim, J.E. An, C.J. Shin, S.E. Seo, S. Jo, J. Kim, S. Ha, H.W. Seo, M.-C. Rho, D.H. Kwon, W.-K. Kim, G. Jeong, J.C. Ryu, J.J. Kim, O.S. Kwon, Second skin as self-protection against γ-hydroxybutyrate, ACS Nano 17 (24) (2023) 25405–25418, http://dx.doi.org/10.1021/acsnano.3c08840, URL https://pubs.acs.org/doi/10.1021/acsnano.3c08840.

[20] L.A. Baumes, M. Buaki Sogo, P. Montes-Navajas, A. Corma, H. Garcia, A colorimetric sensor array for the detection of the date-rape drug γ-hydroxybutyric acid (GHB): A supramolecular approach, Chem. Eur. J. 16 (15) (2010) 4489–4495, http://dx.doi.org/10.1002/chem.200903127, URL https://chemistry-europe.onlinelibrary.wiley.com/doi/10.1002/chem.200903127.

[21] M.P. Elie, M.G. Baron, J.W. Birkett, Enhancement of microcrystalline identification of γ-hydroxybutyrate, J. Forensic Sci. 53 (1) (2008) 147–150, http://dx.doi.org/10.1111/j.1556-4029.2007.00620.x, URL https://onlinelibrary.wiley.com/doi/10.1111/j.1556-4029.2007.00620.x.

[22] M. Germain, B. Desharnais, J. Motard, A. Doyon, C. Bouchard, T. Marcoux, E. Audette, C. Muehlethaler, P. Mireault, On-site drug detection coasters: An inadequate tool to screen for GHB and ketamine in beverages, Forensic Sci. Int. 352 (2023) 111817, http://dx.doi.org/10.1016/j.forsciint.2023.111817, URL https://linkinghub.elsevier.com/retrieve/pii/S0379073823002670.

[23] Y. Shi, X. Cui, M. Shen, P. Xiang, Quantitative analysis of the endogenous GHB level in the hair of the Chinese population using GC/MS/MS, J. Forensic Leg. Med. 39 (2016) 10–15, http://dx.doi.org/10.1016/j.jflm.2016.01.002, URL https://linkinghub.elsevier.com/retrieve/pii/S1752928X16000032.

[24] A.L. Castro, S. Tarelho, M. Dias, F. Reis, H.M. Teixeira, A fast and reliable method for GHB quantitation in whole blood by GC–MS/MS (TQD) for forensic purposes, J. Pharm. Biomed. Anal. 119 (2016) 139–144, http://dx.doi.org/10.1016/j.jpba.2015.11.038, URL https://linkinghub.elsevier.com/retrieve/pii/S0731708515302612.

[25] A.S. Dias, A.L. Castro, P. Melo, S. Tarelho, P. Domingues, J.M. Franco, A fast method for GHB-GLUC quantitation in whole blood by GC–MS/MS (TQD) for forensic purposes, J. Pharm. Biomed. Anal. 150 (2018) 107–111, http://dx.doi.org/10.1016/j.jpba.2017.11.072, URL https://linkinghub.elsevier.com/retrieve/pii/S0731708517327887.

[26] E. Kaufmann, A. Alt, Determination of GHB in urine and serum by LC/MS using a simple one-step derivative, Forensic Sci. Int. 168 (2–3) (2007) 133–137, http://dx.doi.org/10.1016/j.forsciint.2006.07.002, URL https://linkinghub.elsevier.com/retrieve/pii/S0379073806004762.

[27] K.E. Davis, L.D. Hickey, J.V. Goodpaster, Detection of γ-hydroxybutyric acid (GHB) and γ-butyrolactone (GBL) in alcoholic beverages via total vaporization solid-phase microextraction (TV-SPME) and gas chromatography–mass spectrometry, J. Forensic Sci. 66 (3) (2021) 846–853, http://dx.doi.org/10.1111/1556-4029.14660, URL https://onlinelibrary.wiley.com/doi/10.1111/1556-4029.14660.

[28] R.M. Shelby, Techno-physical feminism: anti-rape technology, gender, and corporeal surveillance, Fem. Media Stud. 20 (8) (2020) 1088–1109, http://dx.doi.org/10.1080/14680777.2019.1662823, URL https://www.tandfonline.com/doi/full/10.1080/14680777.2019.1662823.

[29] V.F. Yusuf, N.I. Malek, S.K. Kailasa, Review on metal–organic framework classification, synthetic approaches, and influencing factors: Applications in energy, drug delivery, and wastewater treatment, ACS Omega 7 (49) (2022) 44507–44531, http://dx.doi.org/10.1021/acsomega.2c05310, URL https://pubs.acs.org/doi/10.1021/acsomega.2c05310.

[30] Z. Zong, G. Tian, J. Wang, C. Fan, F. Yang, F. Guo, Recent advances in metal–organic-framework-based nanocarriers for controllable drug delivery and release, Pharmaceutics 14 (12) (2022) 2790, http://dx.doi.org/10.3390/pharmaceutics14122790, URL https://www.mdpi.com/1999-4923/14/12/2790.

[31] G. Cai, X. Ma, M. Kassymova, K. Sun, M. Ding, H.-L. Jiang, Large-scale production of hierarchically porous metal-organic frameworks by a reflux-assisted post-synthetic ligand substitution strategy, ACS Cent. Sci. 7 (8) (2021) 1434–1440, http://dx.doi.org/10.1021/acscentsci.1c00743, URL https://pubs.acs.org/doi/10.1021/acscentsci.1c00743.

[32] F.V. Harzand, S.N.M. Nejad, A. Babapoor, S.M. Mousavi, S.A. Hashemi, A. Gholami, W.-H. Chiang, M.G. Buonomenna, C.W. Lai, Recent advances in metal-organic framework (MOF) asymmetric membranes/composites for biomedical applications, Symmetry 15 (2) (2023) 403, http://dx.doi.org/10.3390/sym15020403, URL https://www.mdpi.com/2073-8994/15/2/403.

[33] B.E. Souza, A.F. Möslein, K. Titov, J.D. Taylor, S. Rudić, J.-C. Tan, Green reconstruction of MIL-100 (Fe) in water for high crystallinity and enhanced guest encapsulation, ACS Sustain. Chem. Eng. 8 (22) (2020) 8247–8255, http://dx.doi.org/10.1021/acssuschemeng.0c01471, URL https://pubs.acs.org/doi/10.1021/acssuschemeng.0c01471.

[34] G. Yuan, L. Tan, P. Wang, Y. Wang, C. Wang, H. Yan, Y.-Y. Wang, MOF-COF composite photocatalysts: Design, synthesis, and mechanism, Cryst. Growth Des. 22 (1) (2022) 893–908, http://dx.doi.org/10.1021/acs.cgd.1c01071, URL https://pubs.acs.org/doi/10.1021/acs.cgd.1c01071.

[35] S. Pal, Y.-Z. Su, Y.-W. Chen, C.-H. Yu, C.-W. Kung, S.-S. Yu, 3D printing of metal–organic framework-based ionogels: Wearable sensors with colorimetric and mechanical responses, ACS Appl. Mater. Interfaces 14 (24) (2022) 28247–28257, http://dx.doi.org/10.1021/acsami.2c02690, URL https://pubs.acs.org/doi/10.1021/acsami.2c02690.

[36] S. Mallakpour, E. Nikkhoo, C.M. Hussain, Application of MOF materials as drug delivery systems for cancer therapy and dermal treatment, Coord. Chem. Rev. 451 (2022) 214262, http://dx.doi.org/10.1016/j.ccr.2021.214262, URL https://linkinghub.elsevier.com/retrieve/pii/S0010854521005361.

[37] J. Winarta, B. Shan, S.M. McIntyre, L. Ye, C. Wang, J. Liu, B. Mu, A decade of UiO-66 research: A historic review of dynamic structure, synthesis mechanisms, and characterization techniques of an archetypal metal-organic framework, Cryst. Growth Des. 20 (2) (2020) 1347–1362, http://dx.doi.org/10.1021/acs.cgd.9b00955.

[38] Y. Wang, J. Yan, N. Wen, H. Xiong, S. Cai, Q. He, Y. Hu, D. Peng, Z. Liu, Y. Liu, Metal-organic frameworks for stimuli-responsive drug delivery, Biomaterials 230 (2020) 119619, http://dx.doi.org/10.1016/j.biomaterials.2019.119619, URL https://linkinghub.elsevier.com/retrieve/pii/S0142961219307185.

[39] K. Hyjek, P.J. Jodłowski, Metal-organic frameworks for efficient drug adsorption and delivery, Sci. Rad. 2 (2) (2023) 117–189, http://dx.doi.org/10.58332/scirad2023v2i2a03, URL https://sci-rad.com/2023v2i2a03/.

[40] P.J. Jodłowski, K. Dymek, G. Kurowski, K. Hyjek, A. Boguszewska-Czubara, B. Budzyńska, W. Mrozek, N. Skoczylas, Ł. Kuterasiński, W. Piskorz, M. Białoruski, R.J. Jędrzejczyk, P. Jeleń, M. Sitarz, Crystal clear: Metal–organic frameworks pioneering the path to future drug detox, ACS Appl. Mater. Interfaces 16 (23) (2024) 29657–29671, http://dx.doi.org/10.1021/acsami.4c02450, URL https://pubs.acs.org/doi/10.1021/acsami.4c02450.

[41] P.J. Jodłowski, K. Dymek, G. Kurowski, K. Hyjek, A. Boguszewska-Czubara, B. Budzyńska, A. Pajdak, Ł. Kuterasiński, W. Piskorz, P. Jeleń, M. Sitarz, In vivo and in vitro studies of efficient mephedrone adsorption over zirconium-based metal-organic frameworks corroborated by DFT+D modeling, Microporous Mesoporous Mater. 359 (2023) 112647, http://dx.doi.org/10.1016/j.micromeso.2023.112647, URL https://linkinghub.elsevier.com/retrieve/pii/S1387181123002184.

[42] K. Hyjek, G. Kurowski, K. Dymek, A. Boguszewska-Czubara, B. Budzyńska, O. Wronikowska-Denysiuk, A. Gajda, W. Piskorz, P. Śliwa, M. Szumera, P. Jeleń, M. Sitarz, P.J. Jodłowski, Metal-organic frameworks for efficient mephedrone detoxification or supervised withdrawal – synthesis, characterisation, and in vivo studies, Chem. Eng. J. 479 (2024) 147655, http://dx.doi.org/10.1016/j.cej.2023.147655, URL https://linkinghub.elsevier.com/retrieve/pii/S1385894723063878.

[43] Q. Zhou, G. Liu, Urea-functionalized MIL-101(Cr)@AC as a new adsorbent to remove sulfacetamide in wastewater treatment, Ind. Eng. Chem. Res. 59 (26) (2020) 12056–12064, http://dx.doi.org/10.1021/acs.iecr.0c01037, URL https://pubs.acs.org/doi/10.1021/acs.iecr.0c01037.

[44] J.R. de Andrade, M.F. Oliveira, M.G.C. da Silva, M.G.A. Vieira, Adsorption of pharmaceuticals from water and wastewater using nonconventional low-cost materials: A review, Ind. Eng. Chem. Res. 57 (9) (2018) 3103–3127, http://dx.doi.org/10.1021/acs.iecr.7b05137, URL https://pubs.acs.org/doi/10.1021/acs.iecr.7b05137.

[45] M. Aghajanzadeh, M. Zamani, H. Molavi, H. Khieri Manjili, H. Danafar, A. Shojaei, Preparation of metal–organic frameworks uio-66 for adsorptive removal of methotrexate from aqueous solution, J. Inorg. Organomet. Polym. Mater. 28 (1) (2018) 177–186, http://dx.doi.org/10.1007/s10904-017-0709-3, URL http://dx.doi.org/10.1007/s10904-017-0709-3.

[46] B.N. Bhadra, I. Ahmed, S. Kim, S.H. Jhung, Adsorptive removal of ibuprofen and diclofenac from water using metal-organic framework-derived porous carbon, Chem. Eng. J. 314 (2017) 50–58, http://dx.doi.org/10.1016/j.cej.2016.12.127.

[47] S. Ghosh, A. Rana, S. Biswas, Metal-organic framework-based fluorescent sensors for the detection of pharmaceutically active compounds, Chem. Mater. 36 (1) (2024) 99–131, http://dx.doi.org/10.1021/acs.chemmater.3c02459, URL https://pubs.acs.org/doi/10.1021/acs.chemmater.3c02459.

[48] P.J. Jodłowski, G. Kurowski, Ł. Kuterasiński, M. Sitarz, P. Jeleń, J. Jaśkowska, A. Kołodziej, A. Pajdak, Z. Majka, A. Boguszewska-Czubara, Cracking the chloroquine conundrum: The application of defective UiO-66 metal-organic framework materials to prevent the onset of heart defects-in vivo and in vitro, ACS Appl. Mater. Interfaces 13 (1) (2021) 312–323, http://dx.doi.org/10.1021/acsami.0c21508, URL https://pubs.acs.org/doi/10.1021/acsami.0c21508.

[49] K. Dymek, G. Kurowski, Ł. Kuterasiński, R.J. Jędrzejczyk, M. Szumera, M. Sitarz, A. Pajdak, Ł. Kurach, A. Boguszewska-Czubara, P.J. Jodłowski, In search of effective UiO-66 metal–organic frameworks for artificial kidney application, ACS Appl. Mater. Interfaces 13 (38) (2021) 45149–45160, http://dx.doi.org/10.1021/acsami.1c05972, URL https://pubs.acs.org/doi/10.1021/acsami.1c05972.

[50] S. Biswas, P.V.D. Voort, A general strategy for the synthesis of functionalised UiO-66 frameworks: Characterisation, stability and CO2 adsorption properties, Eur. J. Inorg. Chem. 2013 (12) (2013) 2154–2160, http://dx.doi.org/10.1002/ejic.201201228, URL https://chemistry-europe.onlinelibrary.wiley.com/doi/10.1002/ejic.201201228.

[51] J. Tang, S. Li, Y. Chu, Y. Xiao, J. Xu, F. Deng, Solid-state NMR studies of the acidity of functionalized metal–organic framework UiO-66 materials, Magn. Reson. Chem. 58 (11) (2020) 1091–1098, http://dx.doi.org/10.1002/mrc.4923, URL https://analyticalsciencejournals.onlinelibrary.wiley.com/doi/10.1002/mrc.4923.

[52] S. Dai, C. Simms, I. Dovgaliuk, G. Patriarche, A. Tissot, T.N. Parac-Vogt, C. Serre, Monodispersed MOF-808 nanocrystals synthesized via a scalable room-temperature approach for efficient heterogeneous peptide bond hydrolysis, Chem. Mater. 33 (17) (2021) 7057–7066, http://dx.doi.org/10.1021/acs.chemmater.1c02174.

[53] P.J. Jodłowski, K. Dymek, G. Kurowski, J. Jaśkowska, W. Bury, M. Pander, S. Wnorowska, K. Targowska-Duda, W. Piskorz, A. Wnorowski, A. Boguszewska-Czubara, Zirconium-based metal-organic frameworks as acriflavine cargos in the battle against coronaviruses-A theoretical and experimental approach, ACS Appl. Mater. Interfaces 14 (25) (2022) 28615–28627, http://dx.doi.org/10.1021/acsami.2c06420, URL https://pubs.acs.org/doi/10.1021/acsami.2c06420.

[54] M.J. Frisch, G. Trucks, H.B. Schlegal, G.E. Scuseria, M.A. Robb, J.R. Cheeseman, G. Scalmani, V. Barone, G.A. Petersson, H. Nakatsuji, X. Li, M. Caricato, A.V. Marenich, J. Bloino, B.G. Janesko, R. Gomperts, B. Mennucci, H.P. Hratchian, J.V. Ortiz, A.F. Izmaylov, J.L. Sonnenberg, D. Williams-Young, F. Ding, F. Lipparini, F. Egidi, J. Goings, B. Peng, A. Petrone, T. Henderson, D. Ranasinghe, V.G. Zakrzewski, J. Gao, N. Rega, G. Zheng, W. Liang, M. Hada, M. Ehra, K. Toyota, R. Fukuda, J. Hasegwa, M. Ishida, T. Nakajima, Y. Hada, O. Kitao, H. Nakai, T. Vreven, K. Throssell, J.A. Montgomery, J.E. Peralta, F. Ogliaro, M.J. Bearpark, J.J. Heyda, E.N. Brothers, K.N. Kudin, V.N. Staroverov, T.A. Keith, R. Kobayashi, J. Normans, K. Raghavachari, A.P. Rendell, J.C. Burant, S.S. Iyengar, J. Tomasi, M. Cossi, J.M. Millam, M. Klene, C. Adamo, R. Cammi, J.W. Otcherski, R.L. Martin, K. Morokuma, O. Farkas, J.B. Foresam, D.J. Fox, Gaussian 16, Revision C.01, Inc., Wallingford CT, 2016.

[55] N. Ferré, M. Filatov, M. Huix-Rotllant, Density-functional methods for excited states, in: Top. Curr. Chem., vol. 368, Springer International Publishing, 2016, http://dx.doi.org/10.1007/978-3-319-22081-9, URL https://link.springer.com/10.1007/978-3-319-22081-9.

[56] M.E. Casida, M. Huix-Rotllant, Many-body perturbation theory (MBPT) and time-dependent density-functional theory (TD-DFT): MBPT insights about what is missing in, and corrections to, the TD-DFT adiabatic approximation, in: N. Ferré, M. Filatov, M. Huix-Rotllant (Eds.), Density-Functional Methods Excit. States, Springer International Publishing, Cham, 2015, pp. 1–60, http://dx.doi.org/10.1007/128_2015_632.

[57] E. Runge, E.K.U. Gross, Density-functional theory for time-dependent systems, Phys. Rev. Lett. 52 (12) (1984) 997–1000, http://dx.doi.org/10.1103/PhysRevLett.52.997, URL https://link.aps.org/doi/10.1103/PhysRevLett.52.997.

[58] A.D. Becke, Density-functional thermochemistry. III. The role of exact exchange, J. Chem. Phys. 98 (7) (1993) 5648–5652, http://dx.doi.org/10.1063/1.464913, arXiv:z0024.

[59] W.R. Wadt, P.J. Hay, Ab initio effective core potentials for molecular calculations. potentials for main group elements Na to Bi, J. Chem. Phys. 82 (1985) 284–298, URL https://api.semanticscholar.org/CorpusID:98167630.

[60] P.J. Hay, W.R. Wadt, Ab initio effective core potentials for molecular calculations. potentials for the transition metal atoms Sc to Hg, J. Chem. Phys. 82 (1) (1985) 270–283, http://dx.doi.org/10.1063/1.448799, URL https://pubs.aip.org/jcp/article/82/1/270/219079/Ab-initio-effective-core-potentials-for-molecular.

[61] S. Miertuš, E. Scrocco, J. Tomasi, Electrostatic interaction of a solute with a continuum. a direct utilizaion of ab initio molecular potentials for the prevision of solvent effects, Chem. Phys. 55 (1) (1981) 117–129, http://dx.doi.org/10.1016/0301-0104(81)85090-2, URL https://linkinghub.elsevier.com/retrieve/pii/0301010481850902.

[62] A. Schaate, P. Roy, A. Godt, J. Lippke, F. Waltz, M. Wiebcke, P. Behrens, Modulated synthesis of Zr-based metal-organic frameworks: From nano to single crystals, Chem. Eur. J. 17 (24) (2011) 6643–6651, http://dx.doi.org/10.1002/chem.201003211.

[63] H. Molavi, M. Zamani, M. Aghajanzadeh, H.K. Manjili, H. Danafar, A. Shojaei, Evaluation of UiO-66 metal organic framework as an effective sorbent for Curcumin's overdose, Appl. Organomet. Chem. 32 (4) (2018) 1–10, http://dx.doi.org/10.1002/aoc.4221, URL https://onlinelibrary.wiley.com/doi/10.1002/aoc.4221.

[64] P. Leo, N. Crespí, C. Palomino, A. Martín, G. Orcajo, G. Calleja, F. Martinez, Catalytic activity and stability of sulfonic-functionalized UiO-66 and MIL-101 materials in Friedel-Crafts acylation reaction, Catal. Today 390–391 (2022) 258–264, http://dx.doi.org/10.1016/j.cattod.2021.10.007, URL https://linkinghub.elsevier.com/retrieve/pii/S0920586121004648.

[65] M. Thommes, K. Kaneko, A.V. Neimark, J.P. Olivier, F. Rodriguez-Reinoso, J. Rouquerol, K.S.W. Sing, Physisorption of gases, with special reference to the evaluation of surface area and pore size distribution (IUPAC technical report), Pure Appl. Chem. 87 (9–10) (2015) 1051–1069, http://dx.doi.org/10.1515/pac-2014-1117, URL https://www.degruyter.com/document/doi/10.1515/pac-2014-1117/html.

[66] J. Xu, J. Liu, Z. Li, X. Wang, Y. Xu, S. Chen, Z. Wang, Optimized synthesis of Zr(IV) metal organic frameworks (MOFs-808) for efficient hydrogen storage, New J. Chem. 43 (10) (2019) 4092–4099, http://dx.doi.org/10.1039/C8NJ06362A, URL https://xlink.rsc.org/?DOI=C8NJ06362A.

[67] M. Bauzá, N. Munar, A. Figuerola, G.T. Palomino, C.P. Cabello, Multifunctional HKUST-1-3D-printed device for the simultaneous extraction of hydrocarbons and dyes from water, J. Water Process. Eng. 58 (2024) 104890, http://dx.doi.org/10.1016/j.jwpe.2024.104890, URL https://linkinghub.elsevier.com/retrieve/pii/S221471442400120X.

[68] M. Bauzá, P. Leo, C.P. Cabello, A. Martin, G. Orcajo, G.T. Palomino, F. Martinez, Catalytic advantages of SO3H-modified UiO-66(Zr) materials obtained via microwave synthesis in friedel-crafts acylation reaction, Inorg. Chem. 63 (38) (2024) 17460–17468, http://dx.doi.org/10.1021/acs.inorgchem.4c01792, URL https://pubs.acs.org/doi/10.1021/acs.inorgchem.4c01792.

[69] Y. Han, M. Liu, K. Li, Y. Zuo, Y. Wei, S. Xu, G. Zhang, C. Song, Z. Zhang, X. Guo, Facile synthesis of morphology and size-controlled zirconium metal-organic framework UiO-66: the role of hydrofluoric acid in crystallization, CrystEngComm 17 (33) (2015) 6434–6440, http://dx.doi.org/10.1039/c5ce00729a.

[70] G.C. Shearer, S. Chavan, S. Bordiga, S. Svelle, U. Olsbye, K.P. Lillerud, Defect engineering: Tuning the porosity and composition of the metal-organic framework UiO-66 via modulated synthesis, Chem. Mater. 28 (11) (2016) 3749–3761, http://dx.doi.org/10.1021/acs.chemmater.6b00602.

[71] K. Dymek, G. Kurowski, K. Hyjek, A. Boguszewska-Czubara, A. Biernasiuk, A. Pajdak, Ł. Kuterasiński, W. Piskorz, M. Gajewska, J. Bała, S. Zapotoczny, P.J. Jodłowski, Metal-organic frameworks@silk composites as efficient levofloxacin carriers against nosocomial infections and pathogens, Appl. Mater. Today 36 (2024) 102044, http://dx.doi.org/10.1016/j.apmt.2023.102044, URL https://linkinghub.elsevier.com/retrieve/pii/S235294072300313X.

[72] J.H. Cavka, S. Jakobsen, U. Olsbye, N. Guillou, C. Lamberti, S. Bordiga, K.P. Lillerud, A new zirconium inorganic building brick forming metal organic frameworks with exceptional stability, J. Am. Chem. Soc. 130 (42) (2008) 13850–13851, http://dx.doi.org/10.1021/ja8057953, URL https://pubs.acs.org/doi/10.1021/ja8057953.

[73] Z. Jin, H. Yang, Exploration of Zr-metal-organic framework as efficient photocatalyst for hydrogen production, Nanoscale Res. Lett. 12 (2017) http://dx.doi.org/10.1186/s11671-017-2311-6.

[74] K. Zhao, Y. Xiang, X. Sun, L. Chen, J. Xiao, X. Liu, Highly efficient one-step conversion of fructose to biofuel 5-ethoxymethylfurfural using a UIO-66-SO3H catalyst, Front. Chem. 10 (2022) 1–8, http://dx.doi.org/10.3389/fchem.2022.900482, URL https://www.frontiersin.org/articles/10.3389/fchem.2022.900482/full.

[75] X.-L. Zhao, M. Shelton, K.-F. Yang, Sulfonic acid-functionalized polyallylamine (sevelamer) as an efficient reusable strong solid acid catalyst for the synthesis of xanthenes derivatives, BMC Chem. 13 (1) (2019) 98, http://dx.doi.org/10.1186/s13065-019-0609-4, URL https://bmcchem.biomedcentral.com/articles/10.1186/s13065-019-0609-4.

[76] A. Bhattacharyya, D. Mondal, I. Roy, G. Sarkar, N.R. Saha, D. Rana, T.K. Ghosh, D. Mandal, M. Chakraborty, D. Chattopadhyay, Studies of the kinetics and mechanism of the removal process of proflavine dye through adsorption by graphene oxide, J. Mol. Liq. 230 (2017) 696–704, http://dx.doi.org/10.1016/j.molliq.2017.01.013, URL https://linkinghub.elsevier.com/retrieve/pii/S0167732216329178.

[77] A.S. Buchelnikov, G.I. Dovbeshko, D.P. Voronin, V.V. Trachevsky, V.V. Kostjukov, M.P. Evstigneev, Spectroscopic study of proflavine adsorption on the carbon nanotube surface, Appl. Spectrosc. 68 (2) (2014) 232–237, http://dx.doi.org/10.1366/13-07205, URL https://journals.sagepub.com/doi/10.1366/13-07205.

[78] M.R. Witkowski, L.A. Ciolino, J.V. DeFrancesco, GHB free acid: II. Isolation and spectroscopic characterization for forensic analysis, J. Forensic Sci. 51 (2) (2006) 330–339, http://dx.doi.org/10.1111/j.1556-4029.2006.00074.x, URL https://onlinelibrary.wiley.com/doi/10.1111/j.1556-4029.2006.00074.x.

[79] D. Gallart-Mateu, M. de la Guardia, S. Garrigues, Date-rape evidence through fast determination of γ-butyrolactone in adulterated beverages, Talanta 232 (2021) 122387, http://dx.doi.org/10.1016/j.talanta.2021.122387, URL https://linkinghub.elsevier.com/retrieve/pii/S0039914021003088.

[80] A.N. Carney, J.J. Newby, Weakly bound complexes of γ-butyrolactone with water as observed in matrix isolation FTIR and theoretical calculations, J. Phys. Chem. A 128 (15) (2024) 2923–2936, http://dx.doi.org/10.1021/acs.jpca.3c07710, URL https://pubs.acs.org/doi/10.1021/acs.jpca.3c07710.

[81] T.J. Ferris, M.J. Went, Synthesis, characterisation and detection of gamma-hydroxybutyrate salts, Forensic Sci. Int. 216 (1–3) (2012) 158–162, http://dx.doi.org/10.1016/j.forsciint.2011.09.014, URL https://linkinghub.elsevier.com/retrieve/pii/S0379073811004610.

[82] P.J. Jodłowski, G. Kurowski, K. Dymek, M. Oszajca, W. Piskorz, K. Hyjek, A. Wach, A. Pajdak, M. Mazur, D.N. Rainer, D. Wierzbicki, P. Jeleń, M. Sitarz, From crystal phase mixture to pure metal-organic frameworks – tuning pore and structure properties, Ultrason. Sonochem. (2023) 106377, http://dx.doi.org/10.1016/j.ultsonch.2023.106377, URL https://linkinghub.elsevier.com/retrieve/pii/S1350417723000895.

[83] J.M. Benevides, J. Kawakami, G.J. Thomas, Mechanisms of drug-DNA recognition distinguished by Raman spectroscopy, J. Raman Spectrosc. 39 (11) (2008) 1627–1634, http://dx.doi.org/10.1002/jrs.2049, URL https://analyticalsciencejournals.onlinelibrary.wiley.com/doi/10.1002/jrs.2049.

[84] A.K. Rappe, C.J. Casewit, K.S. Colwell, W.A. Goddard, W.M. Skiff, UFF, a full periodic table force field for molecular mechanics and molecular dynamics simulations, J. Am. Chem. Soc. 114 (25) (1992) 10024–10035, http://dx.doi.org/10.1021/ja00051a040, URL https://pubs.acs.org/doi/abs/10.1021/ja00051a040.

[85] J. Wyman, The dielectric constant of mixtures of ethyl alcohol and water from -5 to 40°, J. Am. Chem. Soc. 53 (9) (1931) 3292–3301, http://dx.doi.org/10.1021/ja01360a012.

[86] T. Garoma, L. Skidmore, Modeling the influence of ethanol on the adsorption and desorption of selected BTEX compounds on bentonite and kaolin, J. Environ. Sci. 23 (11) (2011) 1865–1872, http://dx.doi.org/10.1016/S1001-0742(10)60653-5, URL https://linkinghub.elsevier.com/retrieve/pii/S1001074210606535.

[87] G.-Y. Li, K.-L. Han, The sensing mechanism studies of the fluorescent probes with electronically excited state calculations, WIREs Comput. Mol. Sci. 8 (2) (2018) http://dx.doi.org/10.1002/wcms.1351, URL https://wires.onlinelibrary.wiley.com/doi/10.1002/wcms.1351.

[88] S. Saffarionpour, S.-Y.S. Tam, L.A.M. van der Wielen, E. Brouwer, M. Ottens, Influence of ethanol and temperature on adsorption of flavor-active esters on hydrophobic resins, Sep. Purif. Technol. 210 (2019) 219–230, http://dx.doi.org/10.1016/j.seppur.2018.05.026, URL https://linkinghub.elsevier.com/retrieve/pii/S1383586618303186.

[89] J. Bossu, N. Le Moigne, S. Corn, P. Trens, F. Di Renzo, Sorption of water–ethanol mixtures by poplar wood: swelling and viscoelastic behaviour, Wood Sci. Technol. 52 (4) (2018) 987–1008, http://dx.doi.org/10.1007/s00226-018-1022-1, URL http://link.springer.com/10.1007/s00226-018-1022-1.

[90] X. Zhao, K. Wang, Z. Gao, H. Gao, Z. Xie, X. Du, H. Huang, Reversing the dye adsorption and separation performance of metal–organic frameworks via introduction of -SO3H groups, Ind. Eng. Chem. Res. 56 (15) (2017) 4496–4501, http://dx.doi.org/10.1021/acs.iecr.7b00128, URL https://pubs.acs.org/doi/10.1021/acs.iecr.7b00128.

[91] T. Xu, M.A. Shehzad, X. Wang, B. Wu, L. Ge, T. Xu, Engineering leaf-like UiO-66-SO3H membranes for selective transport of cations, Nano-Micro Lett. 12 (1) (2020) 51, http://dx.doi.org/10.1007/s40820-020-0386-6, URL http://link.springer.com/10.1007/s40820-020-0386-6.